The Astrophysical Journal Letters, 895:L23 (15pp), 2020 May 20 https://doi.org/10.3847/2041-8213/ab8cc7

A Mildly Relativistic Outflow from the Energetic, Fast-rising Blue Optical Transient CSS161010 in a Dwarf Galaxy

D. L. Coppejans[1], R. Margutti[1,2,36], G. Terreran[1], A. J. Nayana[3,4], E. R. Coughlin[5], T. Laskar[6], K. D. Alexander[1,37], M. Bietenholz[7,8], D. Caprioli[9], P. Chandra[4], M. R. Drout[10,11], D. Frederiks[12], C. Frohmaier[13], K. H Hurley[14], C. S. Kochanek[15,16], M. MacLeod[17], A. Meisner[18], P. E. Nugent[19], A. Ridnaia[12], D. J. Sand[20], D. Svinkin[12], C. Ward[19,21], S. Yang[22,23,24], A. Baldeschi[1], I. V. Chilingarian[17,25], Y. Dong[30], C. Esquivia[1,26], W. Fong[1], C. Guidorzi[27], P. Lundqvist[28,29], D. Milisavljevic[30], K. Paterson[1], D. E. Reichart[31], B. Shappee[32], M. C. Stroh[1], S. Valenti[22], B. A. Zauderer[33,34], and B. Zhang[35]

[1] Center for Interdisciplinary Exploration and Research in Astrophysics (CIERA) and Department of Physics and Astronomy, Northwestern University, Evanston, IL 60208, USA; deanne.coppejans@northwestern.edu
[2] CIFAR Azrieli Global Scholars program, CIFAR, Toronto, Canada
[3] Department of Physics, United Arab Emirates University, Al-Ain, 15551, UAE
[4] National Centre for Radio Astrophysics, Tata Institute of Fundamental Research, P.O. Box 3, Pune, 411007, India
[5] Department of Astrophysical Sciences, Peyton Hall, Princeton University, Princeton, NJ 08544, USA
[6] Department of Physics, University of Bath, Claverton Down, Bath BA2 7AY, UK
[7] Hartebeesthoek Radio Observatory, P.O. Box 443, Krugersdorp, 1740, South Africa
[8] Department of Physics and Astronomy, York University, Toronto, M3J 1P3, Ontario, Canada
[9] Department of Astronomy and Astrophysics, University of Chicago, Chicago, IL 60637, USA
[10] Department of Astronomy and Astrophysics, University of Toronto, 50 St. George Street, Toronto, Ontario, M5S 3H4, Canada
[11] The Observatories of the Carnegie Institution for Science, 813 Santa Barbara St., Pasadena, CA 91101, USA
[12] Ioffe Institute, Polytekhnicheskaya, 26, St. Petersburg, 194021, Russia
[13] Institute of Cosmology and Gravitation, University of Portsmouth, Portsmouth PO1 3FX, UK
[14] University of California at Berkeley, Space Sciences Laboratory, 7 Gauss Way, Berkeley, CA 94720, USA
[15] Center for Cosmology and AstroParticle Physics (CCAPP), The Ohio State University, 191 W. Woodruff Avenue, Columbus, OH 43210, USA
[16] Department of Astronomy Ohio State University, 140 W. 18th Ave., Columbus, OH 43210, USA
[17] Center for Astrophysics—Harvard and Smithsonian, 60 Garden Street, Cambridge, MA 02138, USA
[18] NSF's National Optical-Infrared Astronomy Research Laboratory, 950 N Cherry Ave, Tucson, AZ 85719, USA
[19] Lawrence Berkeley National Laboratory, 1 Cyclotron Road, Berkeley, CA 94720, USA
[20] Steward Observatory, University of Arizona, 933 North Cherry Avenue, Tucson, AZ 85721-0065, USA
[21] Department of Astronomy, University of Maryland, College Park, MD 20742, USA
[22] Department of Physics, University of California, 1 Shields Avenue, Davis, CA 95616-5270, USA
[23] INAF Osservatorio Astronomico di Padova, Vicolo dell'Osservatorio 5, I-35122 Padova, Italy
[24] The Oskar Klein Centre, Department of Astronomy, Stockholm University, AlbaNova, SE-106 91 Stockholm, Sweden
[25] Sternberg Astronomical Institute, M. V. Lomonosov Moscow State University, 13 Universitetsky prospect, Moscow, 119234, Russia
[26] Hamilton College, 198 College Hill Road, Clinton, NY 13323, USA
[27] Department of Physics and Earth Science, University of Ferrara, via Saragat 1, I-44122, Ferrara, Italy
[28] Department of Astronomy, AlbaNova University Center, Stockholm University, SE-10691 Stockholm, Sweden
[29] The Oskar Klein Centre, AlbaNova, SE-10691 Stockholm, Sweden
[30] Department of Physics and Astronomy, Purdue University, 525 Northwestern Avenue, West Lafayette, IN 47907, USA
[31] Department of Physics and Astronomy, University of North Carolina at Chapel Hill, Chapel Hill, NC 27599, USA
[32] Institute for Astronomy, University of Hawai'i, 2680 Woodlawn Drive, Honolulu, HI 96822, USA
[33] National Science Foundation, 2415 Eisenhower Ave., Alexandria, VA 22314, USA
[34] Neils Bohr Institute, University of Copenhagen, Blegdamsvej 17, DK-2100 Copenhagen, Denmark
[35] Department of Physics and Astronomy, University of Nevada, Las Vegas, NV 89154, USA
Received 2020 March 25; revised 2020 April 23; accepted 2020 April 23; published 2020 May 26

Abstract

We present X-ray and radio observations of the Fast Blue Optical Transient CRTS-CSS161010 J045834−081803 (CSS161010 hereafter) at $t = 69$–531 days. CSS161010 shows luminous X-ray ($L_{\rm x} \sim 5 \times 10^{39}$ erg s^{-1}) and radio ($L_{\nu} \sim 10^{29}$ erg s^{-1} Hz^{-1}) emission. The radio emission peaked at ∼100 days post-transient explosion and rapidly decayed. We interpret these observations in the context of synchrotron emission from an expanding blast wave. CSS161010 launched a mildly relativistic outflow with velocity $\Gamma\beta c \geqslant 0.55c$ at ∼100 days. This is faster than the non-relativistic AT 2018cow ($\Gamma\beta c \sim 0.1c$) and closer to ZTF18abvkwla ($\Gamma\beta c \geqslant 0.3c$ at 63 days). The inferred initial kinetic energy of CSS161010 ($E_k \gtrsim 10^{51}$ erg) is comparable to that of long gamma-ray bursts, but the ejecta mass that is coupled to the mildly relativistic outflow is significantly larger (∼0.01–0.1 $M_{\odot}$). This is consistent with the lack of observed γ-rays. The luminous X-rays were produced by a different emission component to the synchrotron radio emission. CSS161010 is located at ∼150 Mpc in a dwarf galaxy with stellar mass $M_* \sim 10^7\,M_{\odot}$ and specific star formation rate sSFR ~ 0.3 Gyr^{-1}. This mass is among the lowest inferred for host galaxies of explosive transients from massive stars. Our observations of CSS161010 are consistent with an engine-driven aspherical explosion from a rare evolutionary path of a H-rich stellar progenitor, but we cannot rule out a stellar tidal disruption event on a centrally located intermediate-mass black hole. Regardless of the physical mechanism, CSS161010 establishes the existence of a new class of rare

[36] Alfred P. Sloan Fellow.
[37] Einstein Fellow.

(rate $< 0.4\%$ of the local core-collapse supernova rate) H-rich transients that can launch mildly relativistic outflows.

Unified Astronomy Thesaurus concepts: Supernovae (1668); Accretion (14); Black holes (162); X-ray transient sources (1852); Radio transient sources (2008)

Supporting material: machine-readable table

1. Introduction

Fast Blue Optical Transients (FBOTs), or alternatively Fast Evolving Luminous Transients, are a class of transients defined by an extremely rapid rise to maximum light (typically <12 days), luminous optical emission ($\gtrsim 10^{43}$ erg s^{-1}), and blue colors. Due to their fast rise-times, they are difficult to detect and have only been identified as a class since the recent advent of high-cadence optical surveys. Only a few tens of systems have been found at optical wavelengths (e.g., Matheson et al. 2000; Ofek et al. 2010; Poznanski et al. 2010; Drout et al. 2013, 2014; Arcavi et al. 2016; Shivvers et al. 2016; Tanaka et al. 2016; Whitesides et al. 2017; Pursiainen et al. 2018; Rest et al. 2018; Tampo et al. 2020). Not all FBOT rise-times and luminosities can be reconciled with standard supernova (SN) models (e.g., Drout et al. 2014), and the diverse properties of the class have led to a range of proposed models. These include explosions of stripped massive stars (e.g., Drout et al. 2013; Moriya et al. 2017), shock breakout emission from an extended low-mass stellar envelope or dense circumstellar medium (CSM; e.g., Ofek et al. 2010; Drout et al. 2014), cooling envelope emission from extended stripped progenitor stars (e.g., Tanaka et al. 2016), helium shell detonations on white dwarfs (Perets et al. 2010; Shen et al. 2010), or scenarios invoking a central engine such as a magnetar or black hole (e.g., Cenko et al. 2012a; Hotokezaka et al. 2017). However, prior to this work, only two FBOTs (AT 2018cow and ZTF18abvkwla) had been detected at radio and/or X-ray wavelengths. The variable X-ray emission (Rivera Sandoval et al. 2018), transient hard X-ray component, steep X-ray decay, and multi-wavelength evolution (Margutti et al. 2019) of AT 2018cow directly indicate a driving central engine (e.g., Prentice et al. 2018; Ho et al. 2019; Kuin et al. 2019; Margutti et al. 2019; Perley et al. 2019). Another direct manifestation of a central engine is the presence of relativistic ejecta; this was recently inferred for ZTF18abvkwla (Ho et al. 2020).

CRTS CSS161010 J045834−081803 (hereafter referred to as CSS161010) was discovered by the Catalina Real-time Transient Survey (Drake et al. 2009) on 2016 October 10. The transient was also detected by the All-Sky Automated Survey for Supernovae (Shappee et al. 2014) and showed a fast $\sim$4 day rise to maximum light at V-band (S. Dong et al. 2020, in preparation). Follow-up optical spectroscopic observations one week later showed a blue and featureless continuum (Reynolds et al. 2016). These characteristics identify CSS161010 as an FBOT (see Drout et al. 2014). Further spectroscopic observations by S. Dong et al. (2020, in preparation), showed broad spectral features (including hydrogen) and placed CSS161010 at a distance of 150 Mpc ($z = 0.034 \pm 0.001$). Optical spectroscopy of the transient host galaxy that we present here leads to $z = 0.0336 \pm 0.0011$, consistent with the estimate above.

In this paper we present radio and X-ray observations of CSS161010 and optical spectroscopic observations of its host galaxy. This paper is organized as follows. In Section 2 we present the observations of CSS161010 and its host galaxy and in Section 3 we infer the blast wave properties based on the radio and X-ray observations. In Sections 4 and 5 we respectively model the host properties and discuss models for CSS161010. Conclusions are drawn in Section 6. The optical observations and spectral evolution will be presented in S. Dong et al. (2020, in preparation). Time is reported relative to the estimated explosion date MJD 57667 (2016 October 6; S. Dong et al. 2020, in preparation). 1σ uncertainties are reported unless stated otherwise (where σ^2 is the variance of the underlying statistical distribution).

2. Observations

2.1. VLA Observations of CSS161010

We observed CSS161010 with the NSF's Karl G. Jansky Very Large Array (VLA) through project VLA/16B-425 and VLA/18A-123 (PI: Coppejans) over five epochs from 2016 December to 2018 March, $\delta t = 69$–530 days after explosion (Table A1 and Figure 1). To monitor the spectral evolution of the source, we observed at mean frequencies of 1.497 (L-band), 3 (S-band), 6.048 (C-band), 10.0 (X-band), and 22.135 GHz (K-band). The bandwidth was divided into 64 (K-band), 32 (X-band) 16 (C-band and S-band), and eight (L-band) spectral windows, each subdivided into 64 2 MHz channels. The observations were taken in standard phase referencing mode, with 3C 147 as a bandpass and flux-density calibrator and QSO J0501–0159 and QSO J0423–0120 as complex gain calibrators.

We calibrated the data using the VLA pipeline in the Common Astronomy Software Applications package (CASA; McMullin et al. 2007) v4.7.2., with additional flagging. For imaging we used Briggs weighting with a robust parameter of 1, and only performed phase-only self-calibration where necessary. We measured the flux density in the image-plane using PyBDSM (Python Blob Detection and Source Measurement; Mohan & Rafferty 2015) with an elliptical Gaussian fixed to the dimensions of the CLEAN beam. To more densely sample the cm-band spectral energy distribution, we subdivided the available bandwidth into 128 MHz sections where possible and imaged each individually. We verified the pipeline reduction by undertaking manual flagging, calibration, imaging, and self-calibration of the first three epochs of VLA observations in CASA. The derived flux densities were consistent with the values measured from the VLA pipeline calibration. We report the flux densities from the VLA pipeline-calibrated data together with a more detailed description of each observation in Table A1. The position that we derive for CSS161010 from these radio observations is R.A. = 04:58:34.396 ± 0.004, decl. = −08:18:03.95 ± 0.03.

2.2. GMRT Observations of CSS161010

We observed CSS161010 for 10 hours with the Giant Metrewave Radio Telescope (GMRT) under the project code DDTB287 (PI: Coppejans). These observations were carried out on 2017 September 14.93, 21.96, 19.88 UT ($\delta t = 344$–351

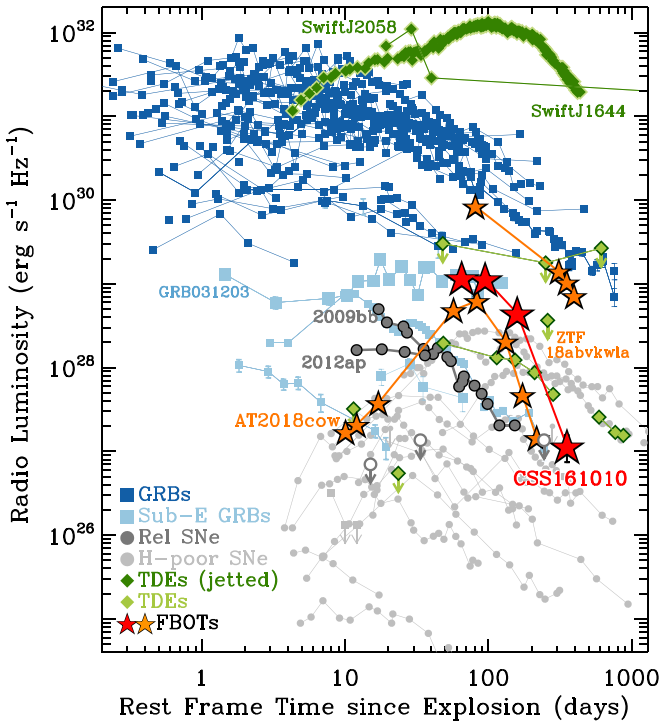

Figure 1. Light curve (8–10 GHz) of CSS161010 (red stars) in the context of those of other classes of explosive transients including gamma-ray bursts (GRBs) (blue squares), sub-energetic GRBs (light-blue squares), relativistic supernovae (SNe) (dark gray circles), normal H-stripped core-collapse SNe (light-gray circles), tidal disruption events (TDEs) (light-green diamonds) and TDEs with relativistic jets (dark-green diamonds). Empty gray circles mark the non-detection of the very rapidly declining SN-Ic 2005ek and the rapidly rising iPTF16asu, which later showed a Ic-BL spectrum (Drout et al. 2013; Whitesides et al. 2017). CSS161010 had a radio luminosity similar to that of the sub-energetic GRB 031203 and higher than that of relativistic SNe, normal SNe, and some sub-energetic GRBs. CSS161010 declined significantly more rapidly than any of these source classes, including the GRBs. The other two Fast Blue Optical Transients with detected radio emission are also shown, with orange stars. References: Berger et al. (2012), Cenko et al. (2012b), Chomiuk et al. (2012), Chandra & Frail (2012), Zauderer et al. (2013), Drout et al. (2013), Chornock et al. (2014), Ho et al. (2019, 2020), Margutti et al. (2013a, 2017b, 2019), Nicholl et al. (2016), Alexander et al. (2016), Brown et al. (2017), Whitesides et al. (2017), Mattila et al. (2018), Eftekhari et al. (2018), D. L. Coppejans et al. (2020, in preparation).

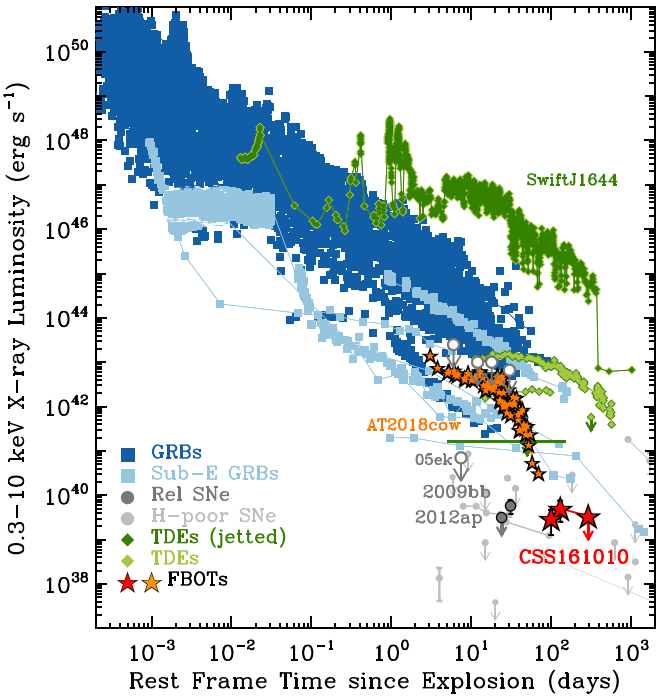

Figure 2. X-ray luminosity (0.3–10 keV) of CSS161010 in the context of those of other classes of transients following the same color scheme as in Figure 1. AT 2018cow is the only other Fast Blue Optical Transient with detected X-ray emission. Empty circles mark the upper limits on the X-ray luminosities of the very rapidly declining type Ic supernova 2005ek, the rapidly rising iPTF16asu, which later showed a Ic-BL spectrum, and the fast-rising, luminous transient "Dougie." References: Margutti et al. (2013a, 2013b, 2019), Drout et al. (2013), Vinkó et al. (2015), Whitesides et al. (2017).

days after explosion) at frequencies 1390, 610, and 325 MHz, respectively (Table A1). The 33 MHz observing bandwidth was split into 256 channels at all three frequencies. We used the Astronomical Image Processing Software to reduce and analyze the data. Specifically, for flagging and calibration we used the FLAGging and CALibration (FLAGCAL) software pipeline developed for GMRT data (Prasad & Chengalur 2012). Additional manual flagging and calibration was also performed. We performed multi-facet imaging to deal with the field which is significantly curved over the GMRT field of view. The number of facets was calculated using the SETFC task. Continuum images were made using the IMAGR task. For each observation we performed a few rounds of phase-only self-calibration and one round of amplitude and phase self-calibration. The errors on the flux density were calculated by adding those given by the task JMFIT and a 15% systematic error in quadrature.

The source positions in our GMRT and VLA images are consistent. To compare the flux density scaling of the VLA and GMRT data, we took an observation at ∼1.49 GHz with each telescope (these observations were separated by two weeks and the central frequencies differed by 0.107 GHz) and the flux densities were consistent. Additionally, we confirmed that the flux density of a known point source in our GMRT 1.4 GHz image was consistent with that quoted in the National Radio Astronomy Observatory (NRAO) VLA Sky Survey (NVSS; Condon et al. 1998) source catalog.

2.3. *Chandra Observations of CSS161010*

We initiated deep X-ray observations of CSS161010 with the Chandra X-ray Observatory on 2017 January 13 under a DDT program (PI Margutti; Program 17508566; IDs 19984, 19985, 19986). Our Chandra observations covered the time range $\delta t \sim 99$–291 days after explosion (Figure 2). The ACIS-S data were reduced with the CIAO software package (v4.9) and relative calibration files, applying standard ACIS data filtering. A weak X-ray source is detected at the location of the optical transient in our first two epochs of observation at $t \sim 99$ days and ∼130 days, while no evidence for X-ray emission is detected at ∼291 days.

In our first observation (ID 19984, exposure time of 29.7 ks) we detect three photons in a 1″ region around the transient, corresponding to a 3.9σ (Gaussian equivalent) confidence-limit detection in the 0.5–8 keV energy range, at a count-rate of $(1.01 \pm 0.58) \times 10^{-4}$ c s^{-1} (the uncertainty here reflects the variance of the underlying Poissonian process). For an assumed power-law spectrum with photon index $\Gamma = 2$ and no intrinsic absorption, the corresponding unabsorbed 0.3–10 keV flux is $F_{\rm x} = (1.33 \pm 0.76) \times 10^{-15}$ erg s^{-1} cm^{-2} and the luminosity is $L_{\rm x} = (3.4 \pm 1.9) \times 10^{39}$ erg s^{-1}. The Galactic neutral

hydrogen column density in the direction of the transient is $NH_{MW} = 4.7 \times 10^{20}$ cm^{-2} (Kalberla et al. 2005).

The X-ray source is still detected at the location of CSS161010 at the time of our second Chandra observation on 2017 February 13 (ID 19985, exposure time of 27.1 ks), with a count-rate of $(1.48 \pm 0.74) \times 10^{-4}$ c s^{-1} and significance of 4.7σ (0.5–8 keV). The corresponding unabsorbed flux is $F_x = (1.94 \pm 0.97) \times 10^{-15}$ erg s^{-1} cm^{-2} (0.3–10 keV), and the luminosity is $L_x = (5.0 \pm 2.5) \times 10^{39}$ erg s^{-1}.

The X-ray emission had faded by the time of our third observation on 2017 July 23 (ID 19986, exposure time of 29.4 ks) and we place a 3σ count-rate upper limit $<1.02 \times 10^{-4}$ c s^{-1} (0.5–8 keV), which corresponds to $F_x < 1.31 \times 10^{-15}$ erg s^{-1} cm^{-2} and $L_x < 3.4 \times 10^{39}$ erg s^{-1} (0.3–10 keV).

2.4. Constraints on the Prompt γ-Ray Emission

We searched for associated prompt γ-ray emission from CSS161010 around the time of explosion with the Inter-Planetary Network (Mars Odyssey, Konus/Wind, INTEGRAL SPI-ACS, Swift-BAT, and Fermi-GBM). Based on the optical photometry of the rise (S. Dong et al. 2020, in preparation), we used a conservative explosion date of JD = 2457669.7 ± 2 for this search. We estimate an upper limit (90% conf.) on the 20–1500 keV fluence of $\sim 8 \times 10^{-7}$ erg cm^{-2} for a burst lasting less than 2.944 s and having a typical Konus Wind short gamma-ray burst (GRB) spectrum (an exponentially cut off power law with $\alpha = -0.5$ and $E_p = 500$ keV). For a typical long GRB spectrum (the Band function with $\alpha = -1$, $\beta = -2.5$, and $E_p = 300$ keV), the corresponding limiting peak flux is $\sim 2 \times 10^{-7}$ erg cm^{-2} s^{-1} (20–1500 keV, 2.944 s scale). The peak flux corresponds to a peak luminosity $L_{pk} < 5 \times 10^{47}$ erg s^{-1}. For comparison, the weakest long GRBs detected have $L_{pk} \approx 10^{47}$ erg s^{-1} (e.g., Nava et al. 2012).

2.5. Host Galaxy Observations

CSS161010 has a faint host galaxy that is visible in deep optical images of the field. The location of CSS161010 is consistent with the inferred center of the host galaxy (R.A. = 04:58:34.398 and decl. = −08:18:04.337, with a separation of 0.″39). We acquired a spectrum of this anonymous host galaxy on 2018 October 10 ($\delta t = 790$ days since explosion) well after the optical transient had completely faded away. We used the Keck Low Resolution Imaging Spectrometer (LRIS) equipped with the 1.″0 slit, the 400/3400 grism for the blue side (6.5 Å resolution) and the 400/8500 grating for the red side (6.9 Å resolution), covering the wavelength range between 3400 and 10200 Å, for a total integration time of 3300 s. The 2D image was corrected for overscan, bias, and flatfields, and the spectrum was then extracted using standard procedures within IRAF.[38] The spectrum was wavelength and flux calibrated using comparison lamps and a standard star observed during the same night and with the same setup. A Galactic extinction $E(B - V) = 0.084$ mag in the direction of the transient was applied (Schlafly & Finkbeiner 2011).

On 2019 February 25, we imaged the field of the host galaxy of CSS161010 in the *VRI* optical bands with Keck+DEIMOS, using an integration time of 720 s for each filter. We used SExtractor (Bertin & Arnouts 1996) to extract the isophotal magnitudes of the host galaxy of CSS161010. We calibrated this photometry using the fluxes of the field stars retrieved from the Pan-STARRS1[39] catalog (Chambers et al. 2016). We converted the *gri* magnitudes of the Pan-STARRS1 field stars to Johnson/Cousins *VRI* magnitudes following Chonis & Gaskell (2008). The final Vega magnitudes of the host of CSS161010 were $V = 21.68 \pm 0.09$ mag, $R = 21.44 \pm 0.07$ mag, $I = 20.91 \pm 0.08$ mag. We then used the same technique to extract *gri* magnitudes of the host from the Pan-STARRS1 data archive images of $g = 21.9 \pm 0.1$ mag, $r = 21.1 \pm 0.1$ mag, and $i = 20.6 \pm 0.1$ mag.

We obtained near-infrared (NIR) imaging of the field of CSS161010 with MMT and the Magellan Infrared Spectrograph (MMIRS; McLeod et al. 2012) in imaging mode on 2018 November 15. We acquired *JHK* images with 60 s exposures for a total integration time of 900 s for *J*, and 1200 s for *H* and *K*. We processed the images using the MMIRS data reduction pipeline (Chilingarian et al. 2015). A separate NIR source is clearly detected at R.A. = 04:58:34.337 decl. = −08:18:04.19, 0.″91 from the radio and optical location of CSS161010 (Figure 3). This source dominates the NIR emission at the location of CSS161010. The inferred Vega measured magnitudes of this contaminating source calibrated against the Two Micron All Sky Survey catalog[40] (Skrutskie et al. 2006) are $J = 19.24 \pm 0.30$ mag, $H = 18.09 \pm 0.08$ mag, $K = 17.76 \pm 0.11$ mag. We note that this source is also detected in the Wide-field Infrared Survey Explorer (WISE) W1 and W2 bands. To measure WISE W1 (3.4 μm) and W2 (4.6 μm) fluxes, we performed point-spread function (PSF) photometry on the Meisner et al. (2018) unWISE coadds. These stacks have a $\sim 4\times$ greater depth than AllWISE, allowing for higher signal-to-noise ratio flux measurements. We infer Vega magnitudes of $W1 = 16.94 \pm 0.07$ and $W2 = 16.74 \pm 0.17$. The uncertainties were estimated via PSF fitting of Monte Carlo image realizations with an appropriate per-pixel noise model. According to Jarrett et al. (2017), W1 − W2 = 0.2 ± 0.2 mag rules out active galactic nuclei, T-dwarfs, and ultra-luminous infrared galaxies. This contaminating source is therefore most likely a foreground star.

3. Inferences from the Radio and X-Ray Observations

3.1. Radio Spectral Evolution and Modeling

The observed radio spectral evolution is consistent with a synchrotron self-absorbed (SSA) spectrum where the self-absorption frequency ν_{sa} evolves to lower frequencies as the ejecta expands and becomes optically thin (Figure 4). The optically thick and thin spectral indices derived from our best-sampled epoch (99 days post explosion) are $\alpha = 2.00 \pm 0.08$ and $\alpha = -1.31 \pm 0.03$, respectively (where $F_\nu \propto \nu^\alpha$). The optically thin flux density scales as $F_\nu \propto \nu^{-(p-1)/2}$, where p is the index of the distribution of relativistic electrons responsible for the synchrotron emission $N_e \propto (\gamma_e)^{-p}$ and γ_e is the Lorentz factor of the electrons (we find $p = 3.6^{+0.4}_{-0.1}$). Table 1 and Figure 4 show the peak frequency ν_p (which is equivalent to the self-absorption frequency ν_{sa}), the peak flux density (F_p), and the parameters derived for the SSA spectrum by fitting each epoch with a broken power law. We find $\nu_p \propto t^{-1.26 \pm 0.07}$ and

[38] http://iraf.noao.edu/

[39] https://panstarrs.stsci.edu

[40] http://www.ipac.caltech.edu/2mass/

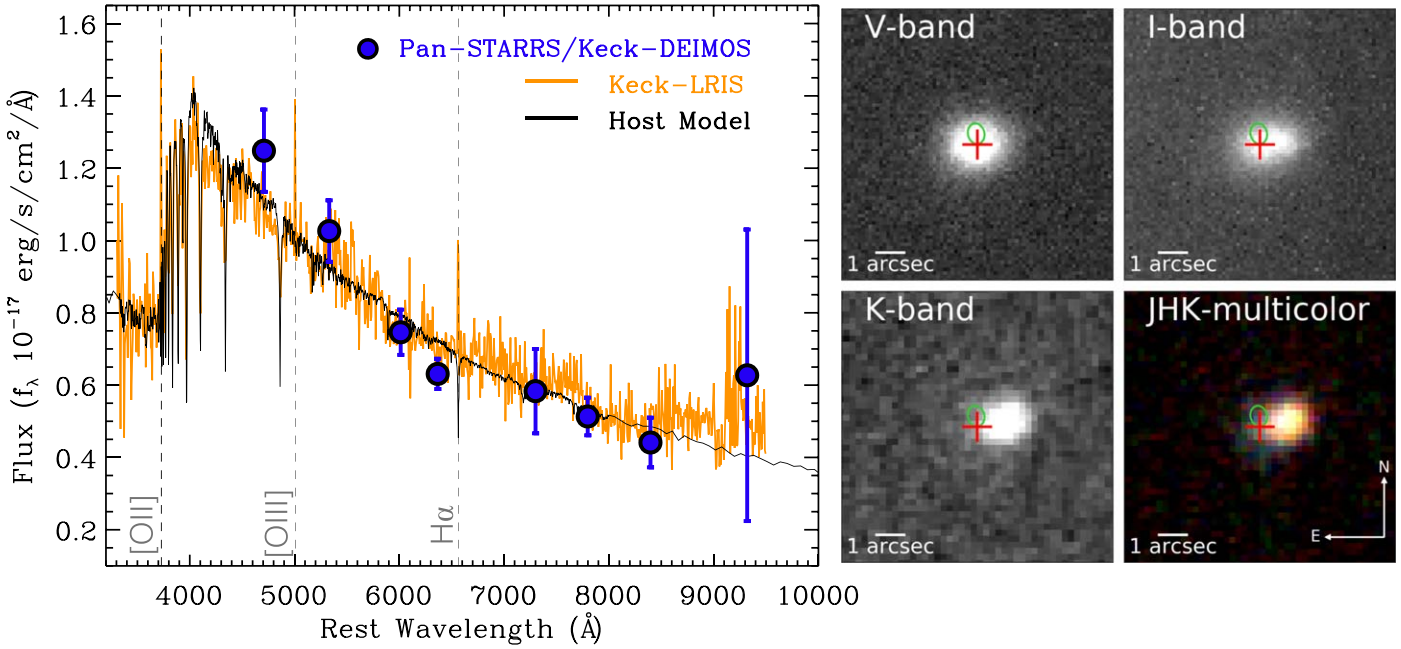

Figure 3. Spectrum, photometry and images of the dwarf galaxy host of CSS161010 at $z = 0.0336 \pm 0.0011$. Left panel: the orange line shows the spectrum of CSS161010's host as observed by Keck/LRIS, while the blue points show the Pan-Starrs/Keck-DEIMOS measurements. The observations have been corrected for a Galactic extinction of $E(B-V) = 0.084$ mag. The Keck/LRIS spectrum has been re-scaled to the Pan-STARRS and Keck/DEIMOS photometry (blue filled circles) as part of the fitting procedure. The black line shows the best-fit FAST model, which has a total stellar mass of $\sim 10^7\ M_\odot$ and current star formation rate $\sim 0.004\ M_\odot\ \mathrm{yr}^{-1}$. Right panels: optical (*V*- and *I*-band from Keck-DEIMOS) and NIR (*JHK*-bands from MMT+MMIRS) images of the surroundings of CSS161010. The red cross marks the position of the centroid of the dwarf host galaxy visible in the *V*-band and the green ellipse marks the 5σ contour of the radio transient at 6 GHz, which is consistent with the optical position of the transient. The apparent shift of the centroid of the emission in the redder bands is due to contamination by a red source (possibly a red dwarf star) almost coincident with the position of the host galaxy of CSS161010. The radio emission is not associated with the contaminating red source.

$F_p \propto t^{-1.79\pm0.09}$ and a steep decay in the radio luminosity of $L_{8\,\mathrm{GHz}} \propto t^{-5.1\pm0.3}$ at >99 days post explosion. The evolution of the SSA peak is consistent with an expanding blast wave, but is different from the evolution of an SSA-dominated, non-strongly decelerating, non-relativistic SN in a wind-like medium where $\nu_p \propto t^{-1}$ and $F_p \sim$ constant (Chevalier 1998; Soderberg et al. 2005, 2006a). The inferred $F_p(t)$ is also steeper than seen in relativistic supernovae (SNe) (see Section 3.3). We compare these properties to the two other radio-detected FBOTs in Section 3.4.

The physical properties of an expanding blast wave can be calculated from an SSA spectrum if F_p, ν_p, the source distance, and the fractions of energy in the relativistic electrons (ϵ_e) and magnetic fields (ϵ_B) in the internal shock are known (Scott & Readhead 1977; Slysh 1990; Readhead 1994; Chevalier 1998; Chevalier & Fransson 2006). We follow the SSA modeling framework for SNe (Chevalier 1998; Chevalier & Fransson 2006) to obtain robust estimates of the blast wave radius R and velocity, environment density n, internal energy U_{int}, and magnetic field B. We employ the subscript "eq" to identify quantities derived under the assumption of equipartition (i.e., $\epsilon_e = \epsilon_B = 1/3$). We emphasize that our estimates of B and R (and subsequently the shock velocity) are only *weakly* dependent on the microphysical parameters. The normalizations of U_{int} and n do depend on the shock microphysics, but the inferred variation of these parameters with time does not. We do not assume any time-dependent evolution for the blast wave, but rather fit each epoch individually to derive the blast wave properties given in Table 1. The relations quoted below were obtained by fitting a power law to these properties over the epochs at 69, 99, and 357 days post explosion. Our major conclusions are not affected if we include our least-constrained epoch (162 days post explosion) in the fits.

3.2. A Mildly Relativistic, Decelerating Blast Wave in a Dense Environment

Over the 308 days spanned by our observations the forward shock radius in CSS161010 expanded according to $R = 3 \times 10^{15} (f\epsilon_e/\epsilon_B)^{-1/19} (t_{\mathrm{obs}}/\mathrm{days})^{0.81\pm0.08}$ cm, where R is calculated from Equation (21) in Chevalier & Fransson (2006), f is the fraction of the spherical volume producing radio emission, and t_{obs} is the time since explosion. In the absence of strong relativistic beaming (which applies to Lorentz factors $\Gamma \gg 1$), the radio emission effectively provides a measure of the blast wave lateral expansion (instead of the radius along our line of sight) or $(\Gamma\beta)c = R/t_{\mathrm{obs}}$, from which we derive an apparent transverse velocity up to 99 days (our best-constrained epoch) of $(\Gamma\beta c)_{\mathrm{eq}} = 0.55 \pm 0.02c$. The blast wave was decelerating during our observations, as at 357 days post explosion we measured $(\Gamma\beta c)_{\mathrm{eq}} = 0.36 \pm 0.04c$. Because of the equipartition assumption and the deceleration of the blast wave, we conclude an initial $\Gamma\beta c > 0.55c$. This result implies a decelerating, mildly relativistic blast wave, with similarities to the radio-loud FBOT event ZTF 18abvkwla (Section 3.4, Ho et al. 2020). We thus conclude that CSS161010 is an FBOT with a mildly relativistic, decelerating outflow, and is the first relativistic transient with hydrogen in its ejecta (optical spectroscopic observations presented in S. Dong et al. 2020, in preparation).

Following the standard Chevalier & Fransson (2006) framework for synchrotron emission from SNe, we further derive an environment density profile

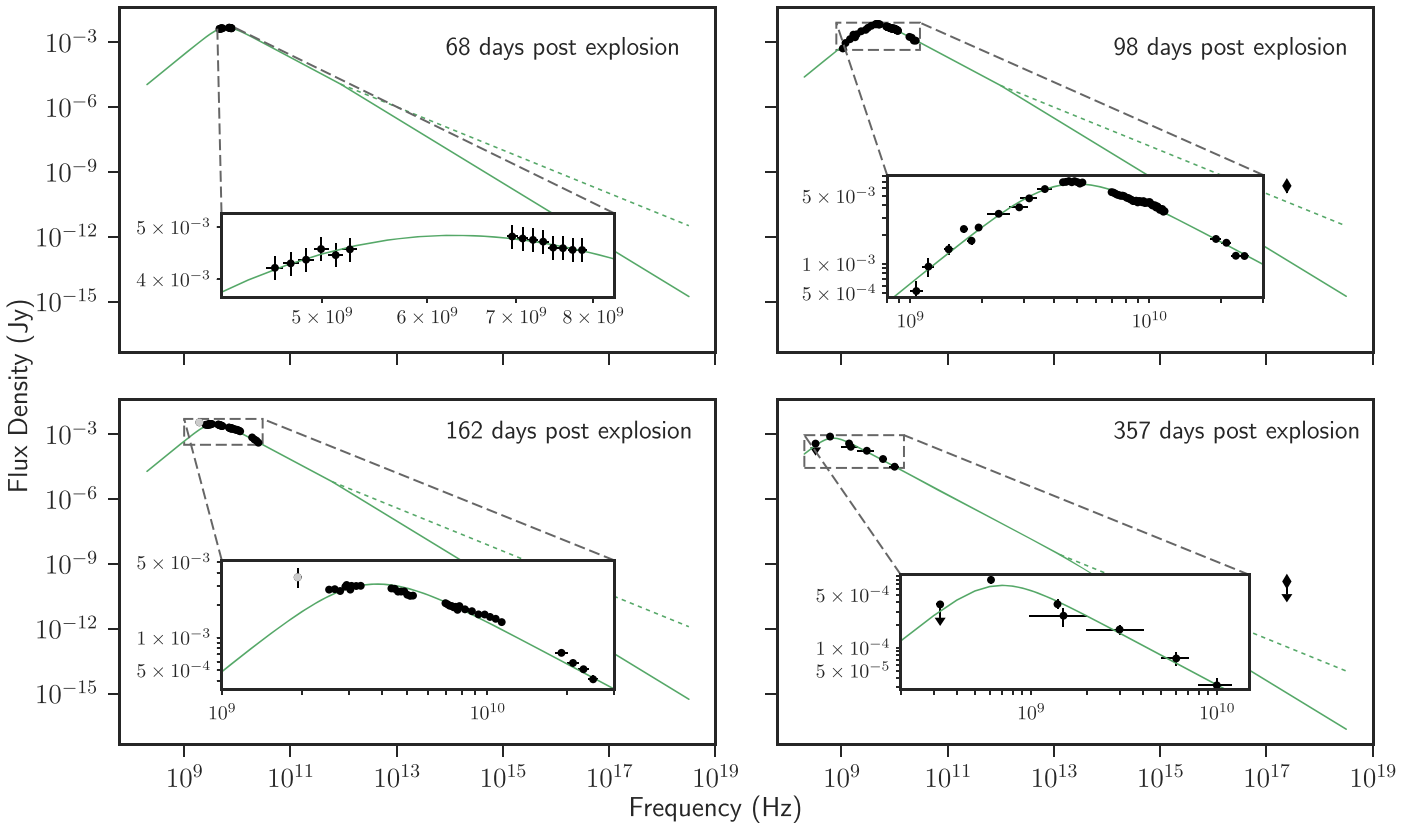

Figure 4. Broadband radio-to-X-ray spectral energy distribution of CSS161010 (black points) along with fits with a synchrotron self-absorbed (SSA) model (green line). The smoothing parameter (−0.9), and optically thick (2.00 ± 0.08) and thin (−1.31 ± 0.03) spectral indices for the fits were derived from our most constraining epoch, at 99 days post explosion. The fitted values are given in Table 1. The measurements below 2 GHz at 162 days post explosion were strongly affected by radio frequency interference and we flagged out much of this band. Subsequently, we treat the lowest frequency point (shown in light gray) with caution. The X-ray emission does not fall on the same SSA spectrum, as the spectral index steepens at frequencies above the cooling break. The dotted (green) line shows the extrapolation of the SSA spectrum without taking the cooling break into account. Note that the X-ray observation in the bottom right panel was taken at 425 days post explosion.

$n = 12\epsilon_B^{-1}(\epsilon_e f/\epsilon_B)^{-8/19}(r/10^{17}\,\mathrm{cm})^{-2.3\pm0.3}\,\mathrm{cm}^{-3}$ at $r_{\rm eq} \geqslant 9.5 \times 10^{16}$ cm. For fiducial microphysics values ($f \approx 0.5$, $\epsilon_e = 0.1$, $\epsilon_B = 0.01$) this result implies $n \approx 700\,\mathrm{cm}^{-3}$ at $r \approx 10^{17}$ cm, corresponding to an effective mass-loss rate of $\dot{M} \approx 2 \times 10^{-4}\,M_\odot\,\mathrm{yr}^{-1}$ for a wind velocity of 1000 km s^{-1}. The inferred environment density is fairly high for massive stars (see Smith 2014) and comparable to the densities inferred for AT 2018cow ($\dot{M} \sim 10^{-4}$–$10^{-3}\,M_\odot\,\mathrm{yr}^{-1}$ Margutti et al. 2019). However, AT 2018cow has a non-relativistic blast wave with $v \sim 0.1c$ and limited (if any) deceleration over the first 150 days (Ho et al. 2019; Margutti et al. 2019; Bietenholz et al. 2020).

If CSS161010 originated from a massive stellar explosion (see Section 5 for discussion) and the radio emission was powered by the interaction of the entire outer stellar envelope with density profile $\rho_{\rm SN} \propto r^{-q}$ with the medium of density $\rho_{\rm CSM} \propto r^{-s}$, we would expect the transient to be still in the "interaction" regime during the time of our radio observations (e.g., Chevalier 1982). During this phase the shock radius expands as $R \propto t^m$ with $m = (q-3)/(q-s)$ (Chevalier 1982), which implies $q \sim 7$ with $s = 2$. It is unclear if the entire outer envelope is contributing to the radio emission or, instead, if the radio-emitting ejecta constitutes a separate ejecta component (as in long GRBs, which have a relativistic jet and a spherical non-relativistic ejecta component associated with the SN). It is thus possible that CSS161010 was already in the energy-conserving limit at $t \sim 100$ days. We discuss below our inferences in this limit.

In the non-relativistic energy-conserving regime the Sedov–Taylor solution applies (ST; von Neumann 1941; Sedov 1946; Taylor 1950) and the shock position scales as $R \propto t^{2/(5-s)}$, from which we would derive $s \sim 2.5$. In the ultra-relativistic $\Gamma \gg 1$ energy-conserving limit the Blandford–McKee solution (Blandford & McKee 1976) applies, $\Gamma \propto R^{(s-3)/2}$ and $dt_{\rm obs} \sim 2dt/\Gamma^2$, from which $R \propto t_{\rm obs}^{1/(4-s)}$, leading to $s \sim 2.7$.[41] The non-relativistic and ultra-relativistic limits, both of which are self-similar, suggest a steep density profile. However, the mildly relativistic nature of the outflow of CSS161010 implies that the blast wave expansion is fundamentally not self-similar, as the speed of light contributes an additional velocity scale that characterizes the expansion of the blast wave (i.e., a velocity scale in addition to the non-relativistic, energy-conserving velocity scaling $V^2 \propto R^{s-3}$). We therefore do not expect the shock position to behave as a simple power law with time, but to instead show some degree of secular evolution as the blast transitions to the non-relativistic regime in which the dependence on the speed of light is lost.

[41] In the discussion of relativistic effects we distinguish between observed time $t_{\rm obs}$ and time in the frame where the blast wave is spherical t. Everywhere else t stands for time in the observer frame.

Table 1
Radio Spectral Properties and Derived Blast Wave Properties

Time[a] (days)	ν_p[b] (GHz)	F_p[b] (mJy)	$R_{\rm eq}$ (10^{16} cm)	$B_{\rm eq}$ (G)	$(\Gamma\beta c)_{\rm eq}$[c] (c)	$U_{\rm eq}$ (10^{49} erg)	$n_{\rm eq}$ (cm^{-3})	$\dot{M}_{\rm eq}$[d] ($10^{-5}\,M_\odot$ yr^{-1})
69	5.6 ± 0.2	8.8 ± 0.2	9.5 ± 0.4	0.38 ± 0.02	0.53 ± 0.02	2.9 ± 0.1	47 ± 5	1.4 ± 0.1
99	4.4 ± 0.1	12.2 ± 0.3	14.1 ± 0.5	0.29 ± 0.01	0.55 ± 0.02	5.6 ± 0.2	25 ± 2	1.7 ± 0.1
357	0.63 ± 0.07	1.2 ± 0.1	33 ± 4	0.052 ± 0.006	0.36 ± 0.04	2.4 ± 0.4	1.9 ± 0.6	0.7 ± 0.2

Notes.
[a] As the observations at 162 days were strongly affected by radio frequency interference at low frequencies and we had to flag most of the data (Figure 4), the optically thick emission was not constrained and we do not include the results for this epoch here or in our modeling. For reference, the derived parameters at 162 days are $F_p = 3.4 \pm 0.1$, $\nu_p = 5.8 \pm 0.1$, $R_{\rm eq} = 12.7 \pm 0.5$, $B_{\rm eq} = 0.241 \pm 0.009$, $(\Gamma\beta c)_{\rm eq} = 0.30 \pm 0.01c$, $U_{\rm int,eq} = 2.9 \pm 0.1$, $n_{\rm eq} = 59 \pm 6$ and $\dot{M}_{\rm eq} = 3.2 \pm 0.2$.
[b] Frequency (column 2) and flux density (column 3) at the intersection of the optically thin and thick synchrotron power laws, from which we calculate the blast wave parameters following Chevalier (1998).
[c] Average apparent velocity $(\Gamma\beta c)_{\rm eq}c = R_{\rm eq}c/t$.
[d] For wind velocity $v_w = 1000$ km s^{-1}.

For mildly relativistic shocks we expect the standard ST scaling to hold up to terms that are proportional to V^2/c^2; Coughlin (2019) showed that the coefficient of proportionality multiplying this correction, σ, is a parameter that depends on the post-shock adiabatic index of the gas (effectively equal to $4/3$) and the ambient density profile (see their Table 1). In particular, following Coughlin (2019) (their Equation (51)), in the mildly relativistic regime the shock velocity varies with position as

$$R^{3-s}\Gamma^2 V^2 = V_i^2(1 + \sigma V^2/c^2), \quad (1)$$

where V_i is the velocity that the shock would have if we ignored relativistic corrections and the shock position is normalized to the time at which the shock sweeps up a comparable amount of rest mass to the initial mass. Inverting and integrating Equation (1) and accounting for $dt_{\rm obs} = (1 - \beta\cos\theta)dt$ (for a patch of the shell at an angle θ with respect to the observer line of sight), it is possible to determine $R(t_{\rm obs})$. An additional complication in the mildly relativistic regime is that the observed emitting surface is viewed at delayed times for different θ; specifically, photons arriving from the poles were radiated earlier than those emitted at the equator (in order to be observed simultaneously) when the ejecta was more relativistic and the radiation was more highly beamed out of our line of sight. Taking the two limiting cases, $dt_{\rm obs} = (1 - V/c)dt$ and $dt_{\rm obs} = dt$, which apply to the early- and late-time evolution, respectively, we find that the environment around CSS161010 was likely steeper than those created by a constant mass-loss rate ($s = 2$), and falls in between the limits provided by the ultra- and non-relativistic regimes. There is some precedent for this non-steady mass loss. Recent observations of a number of SNe show eruptions in the centuries prior to explosion (e.g., Margutti et al. 2014a, 2017a; Smith 2014; Milisavljevic et al. 2015), and AT 2018cow shows a similarly steep density profile (Margutti et al. 2019) to CSS161010. We note that within our framework, a steeper density profile implies that the magnetic field also scales more steeply than the traditional wind scaling of $B \propto R^{-1}$.

3.3. Inferences on the Initial Blast Wave Properties

We determined the shock internal energy $U_{\rm int}$ at each epoch following Chevalier (1998, their Equations (21) and (22)). At 99 days, the equipartition conditions give a robust lower limit of $U_{\rm int} \gtrsim 6 \times 10^{49}$ erg (Table 1), which implies a kinetic energy of $E_k \gtrsim 6 \times 10^{49}$ erg coupled to material with velocity $\Gamma\beta c \geqslant 0.55c$. We compare the shock properties of CSS161010 to those of SNe, FBOTs, and tidal disruption events (TDEs) in Figure 5. The E_k of the fast material in CSS161010 is larger than in normal core-collapse SNe, relativistic SNe,[42] and sub-energetic GRBs, but comparable to GRBs and relativistic TDEs. The shock powering the non-thermal emission in CSS161010 is also significantly faster than in normal SNe, especially considering that it is decelerating and we are

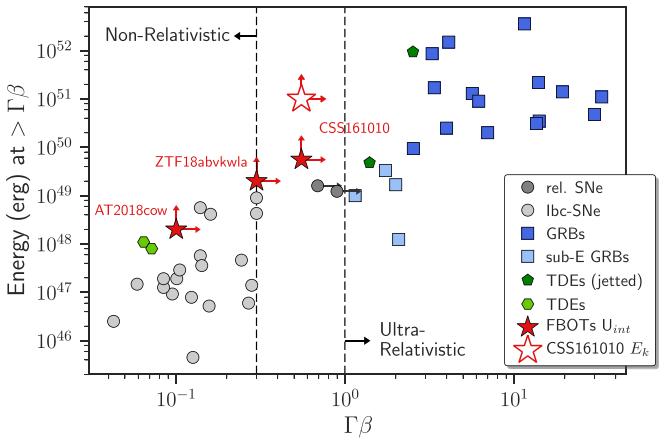

Figure 5. Kinetic energy of the fast-moving material in the outflow with velocities $>\Gamma\beta$ for CSS161010 and other classes of transients, as determined from radio observations. With the exception of the Fast Blue Optical Transients (FBOTs), these properties are measured at approximately 1 day post explosion. We plot the internal energy in the shock ($U_{\rm int}$) for the FBOTs at the time of the observations. For ZTF18abvkwla we calculated this assuming that the 10 GHz measurement at 81 days from (Ho et al. 2020) is the peak of the SSA spectrum as they find a spectral index of -0.16 ± 0.05. For CSS161010 we also plot the kinetic energy at 99 days post explosion/disruption (our best-constrained epoch; see Table 1). The latter is a robust lower limit for the initial kinetic energy. CSS161010 is mildly relativistic and has a velocity at least comparable to that of the relativistic SNe 2009bb (Soderberg et al. 2010b) and 2012ap (Margutti et al. 2014b; Chakraborti et al. 2015). CSS161010 has the fastest outflow of the FBOTs detected to date. References: AT 2018cow (Margutti et al. 2019), ZTF18abvkwla (see footnote 43, Ho et al. 2020), TDEs (Zauderer et al. 2011; Berger et al. 2012; Cenko et al. 2012b; Alexander et al. 2016, 2017), GRBs, and SNe (Margutti et al. 2013a, 2014a) and references therein.

[42] A class of stellar explosions that show mildly relativistic outflows but no detected higher-energy γ-ray counterparts (GRBs) associated with relativistic jets (Soderberg et al. 2010a; Margutti et al. 2014a; Chakraborti et al. 2015; Corsi et al. 2017).

measuring it at a much later phase (≈99 days post explosion) than the SNe shown in Figure 5 at ≈1 day post explosion.

To estimate the initial explosion parameters, we need to extrapolate backwards by assuming a set of blast wave dynamics. Since the early evolution of the blast wave at $t < 70$ days is not constrained by our observations we proceed with robust order-of-magnitude inferences. As the blast wave expands and interacts with the surrounding medium its E_k is converted into $U_{\rm int}$, which implies that the shock's initial E_k is $E_{k,0} > U_{\rm int}$ or $E_{k,0} > 10^{50-51}$ erg for fiducial values $\epsilon_e = 0.1$ and $\epsilon_B = 0.01$. The fact that the shock is decelerating means that the swept-up CSM mass is comparable to or exceeds the mass of the fast material in the blast wave. We can thus estimate the fast ejecta mass and kinetic energy. During our observations the shock wave swept up $M_{\rm sw} \sim 10^{-2}\,M_\odot$ ($\sim 10^{-3}\,M_\odot$ in equipartition) as it expanded from 1×10^{17} to 3×10^{17} cm. The density profile at smaller radii is not constrained, but for profiles ranging from flat to $r^{-2.3}$ we derive a total swept-up mass of $M_{\rm sw} \sim 0.01$–$0.1\,M_\odot$ ($M_{\rm sw} \sim 10^{-3}$–$10^{-2}\,M_\odot$ in equipartition). As the blast wave is decelerating, the mass of the fastest $[(\Gamma\beta c)_{\rm eq} \sim 0.55c]$ ejecta responsible for the non-thermal emission is thus $M_{\rm ej} \sim 0.01$–$0.1\,M_\odot$ and has a kinetic energy of $\sim 10^{51}$–10^{52} erg.

3.4. Comparison to Multi-wavelength FBOTs

CSS161010 and AT 2018cow are the only FBOTs for which we have long-term X-ray *and* radio detections. ZTF18abvkwla is also detected at radio wavelengths (Ho et al. 2020). Remarkably, the radio luminosity of the three FBOTs is large compared to SNe and some sub-energetic GRBs, and is even comparable to the radio emission in long GRBs (ZTF18abvkwla). Even with a sample of three radio-loud FBOTs, we already see a wide range of behaviors, which likely reflects a wide dynamic range of the properties of the fastest outflows of FBOTs.

ZTF18abvkwla and CSS161010 share the presence of mildly relativistic, presumably jetted outflows (Section 5.2.1). ZTF18abvkwla had an expansion velocity[43] (Figure 5) of $\Gamma\beta c \geqslant 0.3c$ at $t \sim 100$ days. They establish a class of transients that are able to launch relativistic ejecta with similarities to GRBs, yet differ from them in their thermal optical emission (and presence of H, for CSS161010; S. Dong et al. 2020, in preparation). The mildly relativistic velocity of CSS161010 and ZTF18abvkwla, and the large energy of the blast wave in CSS161010 differ distinctly from the non-relativistic and slow blast wave in AT 2018cow, which showed $v \sim 0.1c$ (Figure 5, Ho et al. 2019; Margutti et al. 2019). Indeed, high spatial resolution radio observations of AT 2018cow indicated that AT 2018cow did not harbor a long-lived relativistic GRB-like jet (Bietenholz et al. 2020).

The post-peak decline in radio luminosity of the radio-detected FBOTs is extraordinarily steep compared to all other classes of transients (Figure 1), even the energetic and highly collimated GRBs. CSS161010 and AT 2018cow had comparable rates of $L_{8\,\rm GHz} \propto t^{-5.1\pm0.3}$ and $L_{8\,\rm GHz} \propto t^{-4.19\,\pm\,0.4}$ (D. L. Coppejans et al. 2020, in preparation) respectively. The decline of ZTF18abvkwla (Ho et al. 2020) was shallower, with $L_{8\,\rm GHz} \propto t^{-2.7\pm0.4}$. A comparison between the radio properties of these three FBOTs also shows other spectral and evolutionary differences. Compared to AT 2018cow, which had $F_p \propto t^{-1.7\pm0.1}$ and $\nu_p \propto t^{-2.2\pm0.1}$ (Ho et al. 2019; Margutti et al. 2019), CSS161010 exhibited a similar $F_p(t)$ evolution but a slower $\nu_p(t)$ decay. The information on the radio spectral properties of the FBOT ZTF18abvkwla is limited, but we note that at ∼63 days Ho et al. (2020) infer $\nu_p \sim 10$ GHz with a significantly larger radio luminosity $L_\nu \sim 10^{30}$ erg s^{-1} than CSS161010 (Figure 1).

We now turn to the X-ray emission in CSS161010 and AT 2018cow. Although we only have late-time X-ray observations of CSS161010, the luminosity appears to be consistent with that of AT 2018cow at ∼100 days post explosion (see Figure 2). As was the case in AT 2018cow, the source of the X-ray emission cannot be synchrotron emission from the same population of electrons that produces the radio emission. In the two epochs at 99 and 357 days where we have simultaneous X-ray and radio observations, the extrapolated radio flux densities are consistent with the X-ray measurements only if we do not account for the presence of the synchrotron cooling break at $\nu = \nu_c$. For the $B_{\rm eq}$ of Table 1, we expect ν_c to lie between the radio and X-ray bands at $99 < t < 357$ days leading to a flux density steepening $F_\nu \propto \nu^{-p/2} \propto \nu^{-1.8}$ at $\nu > \nu_c$ (Rybicki & Lightman 1979). It follows that the extrapolated SSA spectrum under-predicts the X-ray flux and that another mechanism is thus required to explain the X-ray emission in CSS161010. In AT 2018cow there was also an excess of X-ray emission, which was attributed to a central engine (Prentice et al. 2018; Ho et al. 2019; Kuin et al. 2019; Lyutikov & Toonen 2019; Margutti et al. 2019; Perley et al. 2019). We speculate that the X-ray emission in CSS161010 might also be attributable to the central engine. Interestingly, both FBOTs also have hydrogen-rich outflows (S. Dong et al. 2020, in preparation) and dense environments, and at optical/UV wavelengths are among the most luminous and fastest evolving members of the FBOT family (S. Dong et al. 2020, in preparation).

4. Properties of the Dwarf Host Galaxy

We use the Fitting and Assessment of Synthetic Templates code (FAST; Kriek et al. 2009) to fit the host galaxy emission and constrain the properties of the underlying stellar population. We first combine and re-normalize the Keck-LRIS spectrum by using the broadband PanSTARSS *gri* and DEIMOS *VRI* photometry corrected for Galactic extinction. We do not include the NIR data at $\lambda \geqslant 10000$ Å (i.e., *JHK* and the WISE W1 and W2 bands) in our fits, as these wavelengths are dominated by emission from the contaminating object (Section 2.5). We assume a Chabrier (2003) stellar initial mass function and considered a variety of star formation histories and stellar population libraries. The best-fitting synthetic spectrum, which we show in Figure 3, uses the stellar models of Bruzual & Charlot (2003) with a metallicity of $Z = 0.004$ and no internal extinction ($A_V = 0$ mag), and favors an exponentially declining star formation law yielding a current star formation rate of SFR $\sim 4 \times 10^{-3}\,M_\odot$ yr^{-1}. The total stellar mass of the host galaxy is $M_* \sim 10^7\,M_\odot$, which implies a current specific star formation rate sSFR ~ 0.3 Gyr^{-1}. Other choices of stellar population models, star formation histories, and metallicity produce similar results. For example, using the stellar models of Bruzual & Charlot (2003) and Conroy &

[43] Equation (3) from Ho et al. (2020) should read $\Theta = \frac{\Gamma\beta ct}{d_A(1+z)}$, leading to a revised $\Gamma\beta c > 0.3c$ at $t_{\rm obs} = 81$ days (i.e., ∼63 days rest-frame; A. Ho 2020, private communication).

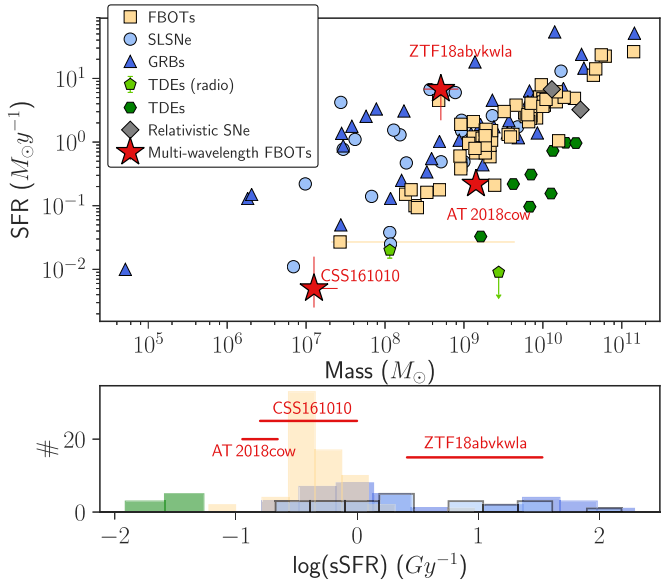

Figure 6. Upper panel: star formation rate (SFR) and stellar mass properties of the dwarf galaxy host of CSS161010 and other radio-loud FBOTs (red stars) in relation to the host galaxies of long GRBs (blue triangles), superluminous SNe (SLSNe) (light-blue circles), FBOTs (squares) and TDEs (green diamonds). Lower panel: histogram of specific SFR (sSFR) for the same classes of transients using the same color coding as above. The dwarf host of CSS161010 has the lowest SFR of the FBOT hosts and a very small stellar mass $M_\star \sim 10^7\,M_\odot$. However, its sSFR is similar to those of other FBOTs, SLSNe, and GRBs. References: AT 2018cow (Perley et al. 2019), ZTF18abvkwla (Ho et al. 2020), TDEs (Holoien et al. 2016; Law-Smith et al. 2017; Saxton et al. 2017 and private communication with Paulina Lira), FBOTs (Drout et al. 2014; Arcavi et al. 2016; Pursiainen et al. 2018), SLSNe I (Lunnan et al. 2014), relativistic SNe (Michałowski et al. 2018), GRBs (Svensson et al. 2010).

Gunn (2010), with either an exponential or delayed exponential star formation history, and considering metallicity values in the range $Z = 0.0008$–0.02 we find $A_V = 0$–0.4 mag, a current stellar age of (0.6–4) Gyr, a stellar mass of $M_* = (1\text{–}3) \times 10^7\,M_\odot$, SFR $= (0.3\text{–}2) \times 10^{-2}\,M_\odot\ \mathrm{yr}^{-1}$, and sSFR $= (0.2\text{–}1)\,\mathrm{Gyr}^{-1}$. The star formation rates that we derive using the [O II] and Hα spectral lines are consistent with the value derived from our models.

Figure 6 shows the properties of CSS161010's host compared to those of the hosts of other relevant classes of explosive transients. Interestingly, CSS161010 has the smallest host mass of the known FBOTs, with the three radio-loud FBOTs known (red stars and symbols) populating the low-mass end of the host galaxy distribution. Hydrogen-stripped superluminous SNe (SLSNe I) and long GRBs also show a general preference for low-mass and low-metallicity hosts (Section 5.2.1 for further discussion). It is important to note that the star formation rate per unit mass of the host of CSS161010 is comparable to that of other transient classes involving massive stars.

We conclude this section by commenting that there is no observational evidence of activity from the dwarf host galaxy nucleus. There were no observed outbursts or flaring events (active galactic nucleus (AGN)-like activity) at the location of CSS161010 prior to explosion. Specifically, we applied the Tractor image modeling code (Lang et al. 2016) across 6 g-band Dark Energy Camera epochs (DECam, from 2018 October 6 to 13) and 137 r-band and 3 g-band Palomar Transient Factory images (PTF, from 2009 October 3 to 2014 November 13) to find the best-fit model for a host galaxy profile and a point source close to the position of CSS161010. We find no evidence for the presence of a variable point source in either DECam (Dey et al. 2019) or PTF images prior to explosion of CSS161010 (2016 October 6).

5. The Intrinsic Nature of CSS161010

The key properties of CSS161010 can be summarized as follows: it had a rise-time of a few days in the optical and showed a large peak optical luminosity of $\sim 10^{44}$ erg s^{-1}. Broad Hα features also indicate that there was hydrogen in the outflow (S. Dong et al. 2020, in preparation). The surrounding CSM has a large density corresponding to an effective mass loss of $\dot{M} \sim 2 \times 10^{-4}\,M_\odot\ \mathrm{yr}^{-1}$ (for $v_w = 1000\,\mathrm{km\,s}^{-1}$) at $r \sim 10^{17}$ cm. The dwarf host galaxy has a stellar mass of $\sim 10^7\,M_\odot$ that is significantly lower than other FBOTs, but has a comparable sSFR (Figure 6). From our radio modeling, we know that the outflow was mildly relativistic with initial $\Gamma\beta c > 0.55c$. The fast outflow has an ejecta mass of $\sim$0.01–0.1 $M_\odot$ and a kinetic energy of $E_k \gtrsim 10^{51}$ erg. The X-ray emission is not produced by the same electrons producing the radio emission.

5.1. Volumetric Rates of the Most Luminous FBOTs in the Local Universe

We present three independent rate estimates for FBOTs such as CSS161010, AT 2018cow, and ZTF18abvkwla, which populate the most luminous end of the optical luminosity distribution of FBOTs with optical bolometric peak luminosity $L_{\mathrm{opt}} \gtrsim 10^{44}$ erg s^{-1}. At the end of this section we compare our estimates to the inferences by Ho et al. (2020) and Tampo et al. (2020), which were published while this work was in an advanced stage of preparation.

Drout et al. (2014) determined an intrinsic rate for FBOTs with absolute magnitude $-16.5 \geqslant M \geqslant -20$ of 4800–8000 events Gpc^{-3} yr^{-1} based on the detection efficiency of the PanSTARRS1 Medium Deep Survey (PS1-MDS) for fast transients as a function of redshift. However, this estimate assumes a Gaussian luminosity function with a mean and variance consistent with the *entire* PS1-MDS population of FBOTs, after correcting for detection volumes. In order to assess the intrinsic rate of *luminous* rapid transients, such as CSS161010, we repeat the rate calculation of Drout et al. (2014), but adopt a new luminosity function based only on the four PS1-MDS events brighter than -19 mag in the g-band (PS1-11qr, PS1-12bbq, PS1-12bv, and PS1-13duy). This yields intrinsic rates for FBOTs with peak magnitudes greater than -19 mag of 700–1400 Gpc^{-3} yr^{-1}, which is $\sim$0.6%–1.2% of the core-collapse SN rate at $z \sim 0.2$ from Botticella et al. (2008) or $\sim$1%–2% of the local (<60 Mpc) core-collapse SN rate from Li et al. (2011b).

We further estimated the luminous FBOT rate from the PTF (Law et al. 2009; Rau et al. 2009). The PTF was an automated optical sky survey that operated from 2009 to 2012 across $\sim$8000 deg^2, with cadences from one to five days, and primarily in the Mould R-band. We adopted the PTF detection efficiencies of Frohmaier et al. (2017) and simulated a population of FBOTs with light curves identical to AT 2018cow (as we have color information for AT 2018cow near optical peak) and a Gaussian luminosity function $M_R = -20 \pm 0.3$ mag. Our methodology closely follows that

Table 2
Volumetric Rate Estimates for the Entire Population of FBOTs (Upper Part) and for the Most Luminous FBOTs (Lower Part)

References	Abs Mag Range at Peak (mag)	Timescale (days)[a]	z	FBOT Rate ($\mathrm{Gpc^{-3}\,yr^{-1}}$)	versus CCSNe[b]	versus SLSNe[c]	versus sub-E GRBs[d]
Drout et al. (2014)	$-20 < M_g < -16.5$	<12	<0.65	4800–8000	7%–11%	2400%–4000%	2100%–3500%
Pursiainen et al. (2018)	$-15.8 < M_g < -22.2$	<10	$0.05 \leqslant z \leqslant 1.56$	$\gtrsim$1000	$\gtrsim$1.4%	$\gtrsim$500%	$\gtrsim$430%
Tampo et al. (2020)	$-17 < M_i < -20$	$\lesssim$15	$0.3 \leqslant z \leqslant 1.5$	$\sim$4000	$\sim$6%	$\sim$2000%	$\sim$1700%
Ho et al. (2020)	$M_g < -20$	<5	$\lesssim$0.1	<560	$<0.8\%$	$<280\%$	$<240\%$
This work (PS1-MDS)	$M_g < -19$	<12	<0.65	700–1400	1%–2%	350%–700%	300%–600%
This work (PTF)	$M_R = -20 \pm 0.3$	$\lesssim$3	$\lesssim$0.1	<300	$<0.4\%$	$<150\%$	$<130\%$

Notes.
[a] Rest frame.
[b] Local universe core-collapse SN rate from Li et al. (2011a) $\mathfrak{R} \sim 70500\ \mathrm{Gpc^{-3}\,yr^{-1}}$.
[c] SLSN rate at $z \sim 0.2$ from Quimby et al. (2013), including type I and type II events $\mathfrak{R} \sim 200\ \mathrm{Gpc^{-3}\,yr^{-1}}$.
[d] Rate of sub-energetic long GRBs before beaming correction from Soderberg et al. (2006b) $\mathfrak{R} \sim 230\ \mathrm{Gpc^{-3}\,yr^{-1}}$.

described in Frohmaier et al. (2018), but with a simulation volume set to $z \leqslant 0.1$ to maintain high completeness. We also performed a search for AT 2018cow-like events in the PTF data and found zero candidates. Given both the results of our simulations and no comparable events in the data, we measure a 3σ upper limit on the luminous FBOTs rate to be 300 $\mathrm{Gpc^{-3}\,yr^{-1}}$, which is $\lesssim$0.25% of the core-collapse SN rate at $z \sim 0.2$ (Botticella et al. 2008) or $\lesssim$0.4% of the local core-collapse SN rate (Li et al. 2011b). This volumetric rate is consistent with what we derive for luminous FBOTs in massive galaxies based on the Distance Less Than 40 Mpc survey (Tartaglia et al. 2018) following Yang et al. (2017). We refer to the PTF rate estimate in the rest of this work.

We compare our rate estimates of luminous FBOTs in the local universe ($z \leqslant 0.1$) with those derived by Ho et al. (2020) from the archival search of 18 months of ZTF-1DC survey. The transient selection criteria by Ho et al. (2020) are comparable to our set-up of the simulations on the PTF data set. Specifically, Ho et al. (2020) selected transients with peak absolute g-band magnitude $M_{g,\mathrm{pk}} < -20$ and rapid rise time <5 days, finding a limiting volumetric rate $<400\,\mathrm{Gpc^{-3}\,yr^{-1}}$ at distances <560 Mpc, consistent with our inferences. Our study and Ho et al. (2020) thus independently identify luminous FBOTs as an intrinsically rare type of transient, with a volumetric rate $<$(0.4–0.6)% the core-collapse SN rate in the local universe. We conclude that luminous FBOTs are sampling a very rare channel of stellar explosion or other rare phenomenon (Section 5.2). Interestingly the luminous FBOT rate is potentially comparable to that of sub-energetic long GRBs ($230^{+490}_{-190}\,\mathrm{Gpc^{-3}\,yr^{-1}}$, 90% c.l., before beaming correction, Soderberg et al. 2006b), and local SLSNe ($199^{+137}_{-86}\,\mathrm{Gpc^{-3}\,yr^{-1}}$ at $z = 0.16$; Quimby et al. 2013).

We end by noting that our rate estimates are *not* directly comparable to those inferred by Tampo et al. (2020) from the HSC-SSP transient survey. These authors considered rapidly evolving transients in a wider range of luminosities ($-17 \geqslant M_i \geqslant -20$) at cosmological distances corresponding to $0.3 \leqslant z \leqslant 1.5$ and inferred a rate $\sim$4000 $\mathrm{Gpc^{-3}\,yr^{-1}}$. A similar argument applies to the FBOT rates by Pursiainen et al. (2018). Table 2 presents a summary of the current estimates of the volumetric rate for both the entire population of FBOTs and for the most luminous FBOTs.

5.2. Physical Models

Multiple physical models have been suggested to explain the optical behavior of FBOTs (see Section 1). Here, we consider mechanisms/transients that could power the radio and X-ray emission of the FBOT CSS161010. As the ejecta is hydrogen-rich (S. Dong et al. 2020, in preparation), we do not consider neutron star mergers and accretion-induced collapse models. We also disfavor models involving the disruption or explosion of white dwarfs (WDs).

CSS161010 is not flaring activity associated with an AGN. The fraction of dwarf galaxies with masses of the order $10^7\,M_\odot$ that host an AGN is not well-constrained (e.g., Mezcua et al. 2018), but as there is at least one AGN host with a stellar mass comparable to CSS161010 ($1\text{–}3 \times 10^7\,M_\odot$; Mezcua et al. 2018), an AGN cannot be excluded based on the small host galaxy mass alone. The evolving synchrotron radio spectrum is not consistent with the typical flat spectrum seen in AGNs. There is also no evidence for prior optical or radio variability in PTF data (Section 4) or the NVSS (Condon et al. 1998). Most importantly, the optical line flux ratios of [N II]λ6584/Hα versus [O III]/λ5007/Hβ (Kewley & Dopita 2002; Kauffmann et al. 2003) from our Keck spectrum (Figure 3) exclude the presence of an AGN.

5.2.1. Stellar Explosion

In Section 3.2 we inferred that CSS161010 has $E_k > 6 \times 10^{49}$ erg coupled to fast-moving material with $\Gamma\beta c \geqslant 0.55c$. This finding implies that the slow-moving material at $v \sim 10{,}000\ \mathrm{km\,s^{-1}}$ would have $E_k > 10^{53}$ erg under the standard scenario of a spherical hydrodynamical collapse of a star, where $E_k \propto (\Gamma\beta)^{-\alpha}$ with $\alpha \approx -5.2$ for a polytropic index of 3 (Tan et al. 2001). This value largely exceeds the $E_k \sim 10^{51}$ erg limit typical of neutrino-powered stellar explosions, pointing to a clear deviation from a spherical collapse. We conclude that if CSS161010 is a stellar explosion, then its fastest outflow component (i.e., the one powering the radio emission that we detected at late times) must have been initially aspherical and potentially jetted, similar to that of GRBs. Indeed, Figure 5 shows that only GRBs (and jetted TDEs) have comparable energy coupled to their relativistic outflows, suggesting that regardless of the exact nature of CSS161010, a compact object (such as a magnetar or accreting black hole) is necessary to explain the energetics of its outflow.

In the context of SNe, CSS161010 thus qualifies as an engine-driven explosion.

This finding has important implications. Shock interaction with, or breakout from, a dense confined shell of material surrounding the progenitor has been proposed to explain the blue optical colors and fast optical evolution of a number of FBOTs (e.g., Drout et al. 2014; Whitesides et al. 2017). Although these mechanisms could explain the optical colors and fast rise times of FBOTs, they cannot naturally produce the mildly relativistic outflows observed in CSS161010 (and ZTFabvkwala, Ho et al. 2020). We thus conclude that a pure shock interaction/breakout scenario of a normal SN shock through a dense medium cannot account for all the properties of luminous FBOTs across the electromagnetic spectrum, and that at least some luminous FBOTs are *also* powered by a central engine, as was inferred for AT 2018cow (Ho et al. 2019; Margutti et al. 2019; Perley et al. 2019). The analysis of ZTF18abvkwla by Ho et al. (2020) supports a similar conclusion.

Known classes of engine-driven stellar explosions include relativistic SNe, (long) GRBs, and SLSNe. The dwarf nature of the host galaxies of luminous FBOTs that are engine-driven (red stars in Figure 6) is reminiscent of that of some SLSNe and GRBs, which show a preference for low-mass galaxies (e.g., Lunnan et al. 2014; Chen et al. 2017; Schulze et al. 2018), as independently pointed out by Ho et al. (2020). A second clear similarity between luminous FBOTs, relativistic SNe and GRBs is the presence of relativistic outflows (Figure 5) and the associated luminous radio emission (Figure 1), which is clearly not present with similar luminosities in SLSNe (Coppejans et al. 2018; Eftekhari et al. 2019; Law et al. 2019).[44] Yet, luminous FBOTs differ from any known class of stellar explosions with relativistic ejecta in two key aspects: (i) the temporal evolution and spectroscopic properties of their thermal UV/optical emission; (ii) CSS161010 showed evidence for a large mass coupled to its fastest (relativistic) outflow. We expand on these major differences below.

Luminous FBOTs with multi-wavelength detections reach optical bolometric peak luminosities $\gtrsim 10^{44}$ erg s^{-1} (Prentice et al. 2018; Margutti et al. 2019; Perley et al. 2019; S. Dong et al. 2020, in preparation) comparable only to SLSNe. The extremely fast temporal evolution (over timescales of ∼days) and hot, mostly featureless initial spectra with $T \sim 40{,}000$ K (Kuin et al. 2019; Margutti et al. 2019; Perley et al. 2019; Ho et al. 2020) distinguish luminous FBOTs from any other engine-driven transients. While it is unclear if the ejecta of ZTF18abvkwla contained hydrogen (Ho et al. 2020), AT 2018cow and CSS161010 showed for hydrogen-rich ejecta (Prentice et al. 2018; Margutti et al. 2019; Perley et al. 2019; S. Dong et al. 2020, in preparation). In fact, CSS161010 is the first case where a relativistic hydrogen-rich outflow is observed, which implies the existence of a new class of engine-driven explosions that originate from progenitors that still retain a significant fraction of their hydrogen envelope at the time of explosion. There are some reasons to expect that jets should be preferentially launched in explosions of hydrogen-stripped progenitors. For example, binary interaction can strip away the stellar envelope while spinning up the core. The angular momentum of the core is an important ingredient for launching jets. Alternatively, jets in hydrogen-rich progenitors could simply lack the necessary energy to pierce the stellar envelope. (e.g., MacFadyen & Woosley 1999; MacFadyen et al. 2001; Bromberg et al. 2011; Lazzati et al. 2012; Nakar & Sari 2012; Margutti et al. 2014b, and references therein).

Next we comment on the amount of mass coupled to the fastest ejecta. While the shock velocity of CSS161010 is comparable to that of the relativistic SNe and the initial E_k of the outflow is similar to GRBs, the fastest ejecta mass of CSS161010 is significantly larger than that of GRB jet outflows, which typically carry $\sim 10^{-6}$–$10^{-5}\,M_\odot$. It thus comes as no surprise that neither on- nor off-axis GRB-like jet models (e.g., Granot & Sari 2002; van Eerten et al. 2012) fit the radio temporal or spectral evolution of CSS161010. Indeed, the ejecta mass carried by GRB jets needs to be small enough to reach sufficiently large velocities to prevent the absorption of γ-rays for pair production (see Dermer et al. 2000; Huang et al. 2002; Nakar & Piran 2003). Explosions with a sufficiently large ejecta mass to be important in the dynamics and absorb the high-energy emission are referred to as "baryon-loaded explosions" or "dirty fireballs." Although predicted (e.g., Huang et al. 2002), such sources have remained fairly elusive. The relativistic SN 2009bb is argued to be relativistic and baryon-loaded with $M_{\rm ej} \geqslant 10^{-2.5}\,M_\odot$ (Chakraborti & Ray 2011), and the transient PTF11agg is another potential relativistic baryon-loaded candidate (Cenko et al. 2013). CSS161010 is mildly relativistic, did not have a detected gamma-ray counterpart (Section 2.4), had a large E_k that is comparable to GRBs, and had an ejecta mass that is intermediate between GRBs and SNe. It is thus a relativistic baryon-loaded explosion or dirty fireball. Interestingly, luminous GRB-like γ-ray emission was also ruled out for the other mildly relativistic FBOT ZTF18abvkwla (Ho et al. 2020).

Our major conclusion is that, while luminous multi-wavelength FBOTs share similarities with other classes of engine-driven explosions, their properties clearly set them apart as a completely new class of engine-driven transients comprising at most a very small fraction of stellar deaths (Section 5.1). Special circumstances are thus needed to create the most luminous FBOTs.

5.2.2. Tidal Disruption Event by an Intermediate-mass Black Hole

One of the proposed models for the FBOT AT 2018cow was a TDE of a star by an intermediate-mass black hole (IMBH; Kuin et al. 2019; Perley et al. 2019). Margutti et al. (2019) disfavor this model as it is difficult to explain the origin of the high-density surrounding medium (inferred from radio observations) with a TDE on an off-center IMBH. CSS161010 is spatially consistent with the nucleus of its host, so this argument is not directly applicable here.

The dwarf host galaxy of CSS161010 is at least ∼10 times less massive than any other confirmed TDE host (Figure 3). The $M_\star \approx 10^7\,M_\odot$ implies that the central BH would likely be an IMBH. The BH masses and occupation fractions in dwarf galaxies are not well constrained. However, using the relations between the BH mass and host galaxy stellar mass in Marleau et al. (2013) and Reines & Volonteri (2015), which were derived largely based on higher-mass galaxies, we obtain a rough estimate for the BH mass of $\sim 10^3\,M_\odot$. For this BH mass,

[44] There is only one SLSN detected to date (Eftekhari et al. 2019; Law et al. 2019) out of the few dozen observed at radio wavelengths (e.g., Coppejans et al. 2018; Law et al. 2019, and references therein). No jet has been detected in an SLSN and for H-stripped SLSNe the radio limits rule out off-axis jets in the lower energy and density range of GRBs (Coppejans et al. 2018).

the X-ray luminosity at ∼100 days is ∼0.01 $L_{\rm Edd}$ (where $L_{\rm Edd}$ is the Eddington luminosity) and the optical bolometric luminosity is 10^3 $L_{\rm Edd}$. The optical luminosity would have to be highly super-Eddington in this scenario. However, the optical luminosity estimate is highly dependent on the assumed temperature, the uncertainty on the BH mass is very large, and CSS161010 was aspherical and clearly showed an outflow. Consequently we cannot conclusively rule out that CSS161010 is a TDE based on the luminosity.

It is similarly not possible to rule out a TDE scenario based on the optical rise and decay timescales. It is true that the optical rise and decay rate of CSS161010 was significantly faster than TDEs on super-massive black holes (SMBHs; e.g., Hinkle et al. 2020). In fact, the ∼4 day optical rise of CSS161010 (S. Dong et al. 2020, in preparation) was shorter than the ∼11 day rise of the fastest TDE discovered to date, iPTF16fnl (which had a BH mass of $\leqslant 10^{6.6}\,M_{\odot}$; Blagorodnova et al. 2017) and formally consistent with the classical TDE scalings $t_{\rm rise} \sim 1.3(M_{\rm BH}/10^3\,M_{\odot})^{1/2}$ days for a Sun-like star disruption. However, the circularization of the debris is unlikely to be efficient and the circularization timescales of the debris are highly uncertain for IMBHs (e.g., Chen & Shen 2018; Darbha et al. 2019) and we cannot directly compare the TDE timescales of SMBHs and IMBHs. The radio and X-ray luminosities of CSS161010 are comparable to those of some jetted TDEs (Figures 1 and 2), although CSS161010 shows a faster radio decline. The kinetic energy is also comparable to the jetted TDEs (Figure 5). In TDEs that lack gamma-ray detections, the radio synchrotron emission is proposed to be from the shock between the CSM and an outflow driven by a super-Eddington accretion phase (e.g., Rees 1988; Strubbe & Quataert 2009; Zauderer et al. 2011; Alexander et al. 2016), or the external shock from the unbound stellar material (Krolik et al. 2016), or internal shocks in a freely expanding relativistic jet (Pasham & van Velzen 2018). The outflows are modeled using equipartition analysis as we have done for CSS161010 in Section 3, so our results are equally applicable to TDE models and we cannot rule out a TDE based on the radio properties.

Based on the aforementioned arguments, and the fact that the dwarf host galaxy spectrum does not have clear post-starburst features, we disfavor the scenario that CSS161010 is a TDE of an IMBH but cannot conclusively exclude it. If this scenario is true, though, then there are several implications. First, as CSS161010 is hydrogen rich (S. Dong et al. 2020, in preparation), the disrupted star would likely not be a WD. Second, CSS161010 would be the TDE with the smallest BH mass to date. This would imply that TDEs on IMBHs can produce transients that launch relativistic outflows and show short rise-times of a few days. If this is the case, then multi-wavelength observations of FBOTs could identify IMBHs and also help to determine the BH mass function and occupation fraction at low galaxy masses. Third, the volumetric rates estimates for SMBH TDEs are ∼200 $\rm Gpc^{-3}\,yr^{-1}$ (K. D. Alexander et al. 2020, in preparation). If the population of luminous FBOTs is the population of TDEs on IMBHs, then our volumetric rate estimate for luminous FBOTs ($\lesssim$300 $\rm Gpc^{-3}\,yr^{-1}$) would imply that the rate of TDEs on IMBHs would be at most that of the TDE rate of SMBHs.

6. Summary and Conclusions

We present X-ray and radio observations of the luminous FBOT CSS161010 and its dwarf host galaxy. The optical properties of the transient are described in S. Dong et al. (2020, in preparation). At a distance of ∼150 Mpc, CSS161010 is the second closest FBOT (after AT 2018cow). To date, CSS161010 is one of only two FBOTs detected at radio *and* X-ray wavelengths (including AT 2018cow; Rivera Sandoval et al. 2018; Ho et al. 2019; Margutti et al. 2019) and three detected at radio wavelengths (including AT 2018cow and ZTF18abvkwla, Ho et al. 2020).

We highlight below our major observational findings.

1. CSS161010 reached a radio luminosity $L_{\nu} \sim 10^{29}$ $\rm erg\,s^{-1}\,Hz^{-1}$ (at $\nu = 6$ GHz) comparable to sub-energetic GRBs (i.e., significantly larger than normal SNe), with a steep after-peak temporal decline similar to that observed in AT 2018cow.
2. The radio properties of CSS161010 imply the presence of a decelerating mildly relativistic outflow with $\Gamma\beta c > 0.55c$ at $t = 99$ days, carrying a large ejecta mass $\gtrsim 0.01\,M_{\odot}$ and kinetic energy $E_k > 10^{50}$ erg, and propagating into a dense environment with $n \approx 700\,\rm cm^{-3}$ at $r \approx 10^{17}$ cm (an effective mass-loss rate of $\dot{M} \approx 2 \times 10^{-4}\,M_{\odot}\,\rm yr^{-1}$ for a wind velocity of $1000\,\rm km\,s^{-1}$).
3. The X-ray luminosity of $3 \times 10^{39}\,\rm erg\,s^{-1}$ (at 99 days) is too bright to be synchrotron emission from the same population of electrons powering the radio emission. In AT 2018cow this X-ray excess was attributed to a central engine and we speculate that this is also the case in CSS161010.
4. CSS161010 resides in a small dwarf galaxy with stellar mass $M_{*} \sim 10^7\,M_{\odot}$ (the smallest host galaxy to an FBOT to date). However, its specific star formation rate, $\rm sSFR = (0.2–1)\,Gyr^{-1}$, is comparable to other transient host galaxies (e.g., GRBs and SLSNe). Intriguingly, all the FBOTs with multi-wavelength detections so far have dwarf host galaxies (Prentice et al. 2018; Perley et al. 2019; Ho et al. 2020).
5. CSS161010, AT 2018cow, and ZTF18abvkwla belong to a rare population of luminous FBOTs ($M_R < -20$ mag at peak). For this population, using PTF data, we estimate a volumetric rate $<300\,\rm Gpc^{-3}\,yr^{-1}$, which is $\lesssim$0.4% of the local core-collapse SN rate. This result is consistent with the estimates by Ho et al. (2020). We thus reach the same conclusion as Ho et al. (2020) that luminous FBOTs stem from a rare progenitor pathway.

In the context of stellar explosions, the properties of CSS161010 imply a clear deviation from spherical symmetry (as in the case of GRB jets), and hence the presence of a "central engine" (black hole or neutron star) driving a potentially collimated mildly relativistic outflow. Differently from GRBs, CSS161010 (i) has a significantly larger mass coupled to the relativistic outflow, which is consistent with the lack of detected γ-rays, and (ii) the ejecta is hydrogen-rich (S. Dong et al. 2020, in preparation). For CSS161010 we cannot rule out the scenario of a stellar tidal disruption on an IMBH. However we note that this scenario would imply a highly super-Eddington accretion rate of $\sim 10^3\,L_{\rm edd}$ for our (uncertain) BH mass estimate $\sim 10^3\,M_{\odot}$. Irrespective of the

exact nature of CSS161010, CSS161010 establishes a new class of hydrogen-rich, mildly relativistic transients.

We end with a final consideration. The three known FBOTs that are detected at radio wavelengths are among the most luminous and fastest-rising among FBOTs in the optical regime (Ho et al. 2019, 2020; Margutti et al. 2019; Perley et al. 2019; S. Dong et al. 2020, in preparation). Intriguingly, all the multi-wavelength FBOTs also have evidence for a compact object powering their emission (e.g., Prentice et al. 2018; Ho et al. 2019; Kuin et al. 2019; Margutti et al. 2019; Perley et al. 2019). We consequently conclude, independently of (but consistently with) Ho et al. (2020), that at least some luminous FBOTs must be engine-driven and cannot be accounted for by existing FBOT models that do not invoke compact objects to power their emission across the electromagnetic spectrum. Furthermore, even within this sample of three luminous FBOTs with multiwavelength observations, we see a wide diversity of properties of their fastest ejecta. While CSS161010 and ZTF18abvkwla harbored mildly relativistic outflows, AT 2018cow is instead non-relativistic. Radio and X-ray observations are critical to understanding the physics of this intrinsically rare and diverse class of transients.

We thank the anonymous referee for their feedback. We also thank the entire Chandra team, the VLA, and the GMRT for their work, time, and dedication that made these observations possible. We also thank Subo Dong, Brian Metzger, Kris Stanek, Cliff Johnson, Rocco Coppejans, Todd Thompson, and Giacomo Fragione for useful discussions and comments. The Margutti's team at Northwestern is partially funded by the Heising-Simons Foundation under grant # 2018-0911 (PI: Margutti) and by NASA Grant #80NSSC19K0384. R.M. acknowledges support by the National Science Foundation under Award No. AST-1909796. W.M. Keck Observatory and MMT Observatory access was supported by Northwestern University and the Center for Interdisciplinary Exploration and Research in Astrophysics (CIERA). Raffaella Margutti is a CIFAR Azrieli Global Scholar in the Gravity & the Extreme Universe Program, 2019. This research was supported in part by the National Science Foundation under grant No. NSF PHY-1748958. K.D.A. and E.R.C. acknowledge support provided by NASA through the Hubble Fellowship Program, grants HST-HF2-51403.001 and HST-HF2-51433.001-A, awarded by the Space Telescope Science Institute, which is operated by the Association of Universities for Research in Astronomy, Inc., for NASA, under contract NAS5-26555. C.S. K. is supported by NSF grants AST-1908952 and AST-1814440. Research by D.J.S. is supported by NSF grants AST-1821967, 1821987, 1813708, 1813466, and 1908972. T.A.T. is supported in part by NASA Grant #80NSSC18K0526. B.J.S. is supported by NSF grants AST-1908952, AST-1920392, and AST-1911074. M.R.D. acknowledges support from the Dunlap Institute at the University of Toronto and the Canadian Institute for Advanced Research (CIFAR). B.A.Z. acknowledges support from the DARK Cosmology Centre and while serving at the National Science Foundation. D.S., D.F., and A.R. gratefully acknowledge support from RFBR grant 18-02-00062. The National Radio Astronomy Observatory is a facility of the National Science Foundation operated under cooperative agreement by Associated Universities, Inc. GMRT is run by the National Centre for Radio Astrophysics of the Tata Institute of Fundamental Research. The scientific results reported in this paper are based in part on observations made by the Chandra X-ray Observatory. This research has made use of software provided by the Chandra X-ray Center (CXC) in the application packages CIAO. The data presented herein were obtained at the W. M. Keck Observatory, which is operated as a scientific partnership among the California Institute of Technology, the University of California and the National Aeronautics and Space Administration. The Observatory was made possible by the generous financial support of the W. M. Keck Foundation. The authors wish to recognize and acknowledge the very significant cultural role and reverence that the summit of Maunakea has always had within the indigenous Hawaiian community. We are most fortunate to have the opportunity to conduct observations from this mountain. The Pan-STARRS1 Surveys (PS1) and the PS1 public science archive have been made possible through contributions by the Institute for Astronomy, the University of Hawaii, the Pan-STARRS Project Office, the Max-Planck Society and its participating institutes, the Max Planck Institute for Astronomy, Heidelberg and the Max Planck Institute for Extraterrestrial Physics, Garching, The Johns Hopkins University, Durham University, the University of Edinburgh, the Queen's University Belfast, the Harvard-Smithsonian Center for Astrophysics, the Las Cumbres Observatory Global Telescope Network Incorporated, the National Central University of Taiwan, the Space Telescope Science Institute, the National Aeronautics and Space Administration under grant No. NNX08AR22G issued through the Planetary Science Division of the NASA Science Mission Directorate, the National Science Foundation grant No. AST-1238877, the University of Maryland, Eotvos Lorand University (ELTE), the Los Alamos National Laboratory, and the Gordon and Betty Moore Foundation. This publication makes use of data products from the Wide-field Infrared Survey Explorer, which is a joint project of the University of California, Los Angeles, and the Jet Propulsion Laboratory/California Institute of Technology, funded by the National Aeronautics and Space Administration. The CSS survey is funded by the National Aeronautics and Space Administration under grant No. NNG05GF22G issued through the Science Mission Directorate Near-Earth Objects Observations Program. The CRTS survey is supported by the U.S. National Science Foundation under grants AST-0909182 and AST-1313422. Research by D.J.S. is supported by NSF grants AST-1821987 and 1821967. Research by S.V. is supported by NSF grants AST-1813176. I.C.'s research is supported by the Smithsonian Astrophysical Observatory Telescope Data Center, the Russian Science Foundation grant 19-12-00281 and the Program of development at M.V. Lomonosov Moscow State University through the Leading Scientific School "Physics of stars, relativistic objects and galaxies." This publication makes use of the Interplanetary Network Master Burst List at ssl.berkeley.edu/ipn3/masterli.html.

Appendix
Observations

Table A1 lists the details and measured flux densities of our VLA observations. The flux densities obtained by dividing the bandwidth into finer frequency bins are available online.

Table A1
Radio Observations of CSS161010

Start Date (UT)	Time[a] (days)	Frequency[b] (GHz)	Bandwidth (GHz)	Flux Density[c] (mJy)	Telescope
2016 Dec 14	69	6.10	2.048	4.5 ± 0.2	VLA
2017 Jan 13	99	1.50	1.024	1.5 ± 0.1	VLA
2017 Jan 13	99	3.00	2.048	4.3 ± 0.2	VLA
2017 Jan 13	99	6.10	2.048	6.1 ± 0.3	VLA
2017 Jan 13	99	9.87	4.096	4.2 ± 0.2	VLA
2017 Mar 17	162	1.50	1.024	4.7 ± 0.6[d]	VLA
2017 Mar 17	162	2.94	2.048	2.9 ± 0.2	VLA
2017 Mar 17	162	6.10	2.048	2.3 ± 0.1	VLA
2017 Mar 17	162	9.74	4.096	1.74 ± 0.09	VLA
2017 Mar 17	162	22.00	8.192	0.56 ± 0.03	VLA
2017 Sep 14	343	1.39	0.032	0.38 ± 0.05	GMRT
2017 Sep 19	348	0.33	0.032	$\leqslant$0.375	GMRT
2017 Sep 21	350	0.61	0.032	0.79 ± 0.09	GMRT
2017 Sep 28	357	1.50	1.024	0.27 ± 0.07	VLA
2017 Sep 28	357	3.00	2.048	0.17 ± 0.03	VLA
2017 Sep 28	357	6.05	2.048	0.07 ± 0.01	VLA
2017 Sep 28	357	10.00	4.096	0.032 ± 0.008	VLA
2018 Mar 21	531	1.50	1.024	$\leqslant$0.065	VLA
2018 Mar 21	531	10.00	4.096	$\leqslant$0.018	VLA

Notes.
[a] Days since JD 2457668.
[b] The table containing flux densities for each of the sub-bands as displayed in Figure 4 is available online.
[c] Uncertainties are quoted at 1σ, and upper limits are quoted at 3σ. The errors take a systematic uncertainty of 5% (VLA) or 15% (GMRT) into account.
[d] There was significant radio frequency interference in this band.

(This table is available in its entirety in machine-readable form.)

ORCID iDs

D. L. Coppejans https://orcid.org/0000-0001-5126-6237
R. Margutti https://orcid.org/0000-0003-4768-7586
G. Terreran https://orcid.org/0000-0003-0794-5982
A. J. Nayana https://orcid.org/0000-0002-8070-5400
E. R. Coughlin https://orcid.org/0000-0003-3765-6401
T. Laskar https://orcid.org/0000-0003-1792-2338
K. D. Alexander https://orcid.org/0000-0002-8297-2473
M. Bietenholz https://orcid.org/0000-0002-0592-4152
D. Caprioli https://orcid.org/0000-0003-0939-8775
P. Chandra https://orcid.org/0000-0002-0844-6563
M. R. Drout https://orcid.org/0000-0001-7081-0082
D. Frederiks https://orcid.org/0000-0002-1153-6340
C. Frohmaier https://orcid.org/0000-0001-9553-4723
K. H Hurley https://orcid.org/0000-0003-3315-1975
C. S. Kochanek https://orcid.org/0000-0001-6017-2961
M. MacLeod https://orcid.org/0000-0002-1417-8024
A. Meisner https://orcid.org/0000-0002-1125-7384
P. E. Nugent https://orcid.org/0000-0002-3389-0586
D. J. Sand https://orcid.org/0000-0003-4102-380X
D. Svinkin https://orcid.org/0000-0002-2208-2196
S. Yang https://orcid.org/0000-0002-2898-6532
I. V. Chilingarian https://orcid.org/0000-0002-7924-3253
Y. Dong https://orcid.org/0000-0002-9363-8606
W. Fong https://orcid.org/0000-0002-7374-935X
C. Guidorzi https://orcid.org/0000-0001-6869-0835
P. Lundqvist https://orcid.org/0000-0002-3664-8082
D. Milisavljevic https://orcid.org/0000-0002-0763-3885
K. Paterson https://orcid.org/0000-0001-8340-3486
D. E. Reichart https://orcid.org/0000-0002-5060-3673
B. Shappee https://orcid.org/0000-0003-4631-1149
M. C. Stroh https://orcid.org/0000-0002-3019-4577
S. Valenti https://orcid.org/0000-0001-8818-0795
B. Zhang https://orcid.org/0000-0002-9725-2524

References

Alexander, K. D., Berger, E., Guillochon, J., Zauderer, B. A., & Williams, P. K. G. 2016, ApJL, 819, L25
Alexander, K. D., Wieringa, M. H., Berger, E., Saxton, R. D., & Komossa, S. 2017, ApJ, 837, 153
Arcavi, I., Wolf, W. M., Howell, D. A., et al. 2016, ApJ, 819, 35
Berger, E., Zauderer, A., Pooley, G. G., et al. 2012, ApJ, 748, 36
Bertin, E., & Arnouts, S. 1996, A&AS, 117, 393
Bietenholz, M. F., Margutti, R., Coppejans, D., et al. 2020, MNRAS, 491, 4735
Blagorodnova, N., Gezari, S., Hung, T., et al. 2017, ApJ, 844, 46
Blandford, R. D., & McKee, C. F. 1976, PhFl, 19, 1130
Botticella, M. T., Riello, M., Cappellaro, E., et al. 2008, A&A, 479, 49
Bromberg, O., Nakar, E., & Piran, T. 2011, ApJL, 739, L55
Brown, G. C., Levan, A. J., Stanway, E. R., et al. 2017, MNRAS, 472, 4469
Bruzual, G., & Charlot, S. 2003, MNRAS, 344, 1000
Cenko, S. B., Bloom, J. S., Kulkarni, S. R., et al. 2012a, MNRAS, 420, 2684
Cenko, S. B., Krimm, H. A., Horesh, A., et al. 2012b, ApJ, 753, 77
Cenko, S. B., Kulkarni, S. R., Horesh, A., et al. 2013, ApJ, 769, 130
Chabrier, G. 2003, PASP, 115, 763
Chakraborti, S., & Ray, A. 2011, ApJ, 729, 57
Chakraborti, S., Soderberg, A., Chomiuk, L., et al. 2015, ApJ, 805, 187
Chambers, K. C., Magnier, E. A., Metcalfe, N., et al. 2016, arXiv:1612.05560
Chen, J.-H., & Shen, R.-F. 2018, ApJ, 867, 20
Chen, T.-W., Smartt, S. J., Yates, R. M., et al. 2017, MNRAS, 470, 3566
Chevalier, R. A. 1982, ApJ, 259, 302
Chevalier, R. A. 1998, ApJ, 499, 810
Chevalier, R. A., & Fransson, C. 2006, ApJ, 651, 381
Chilingarian, I., Beletsky, Y., Moran, S., et al. 2015, PASP, 127, 406
Chomiuk, L., Soderberg, A., Margutti, R., et al. 2012, ATel, 3931, 1
Chonis, T. S., & Gaskell, C. M. 2008, AJ, 135, 264
Chornock, R., Berger, E., Gezari, S., et al. 2014, ApJ, 780, 44

Condon, J. J., Cotton, W. D., Greisen, E. W., et al. 1998, AJ, 115, 1693
Conroy, C., & Gunn, J. E. 2010, ApJ, 712, 833
Coppejans, D. L., Margutti, R., Guidorzi, C., et al. 2018, ApJ, 856, 56
Corsi, A., Cenko, S. B., Kasliwal, M. M., et al. 2017, ApJ, 847, 54
Coughlin, E. R. 2019, ApJ, 880, 108
Darbha, S., Coughlin, E. R., Kasen, D., & Nixon, C. 2019, MNRAS, 488, 5267
Dermer, C. D., Chiang, J., & Mitman, K. E. 2000, ApJ, 537, 785
Dey, A., Schlegel, D. J., Lang, D., et al. 2019, AJ, 157, 168
Drake, A. J., Djorgovski, S. G., Mahabal, A., et al. 2009, ApJ, 696, 870
Drout, M. R., Chornock, R., Soderberg, A. M., et al. 2014, ApJ, 794, 23
Drout, M. R., Soderberg, A. M., Mazzali, P. A., et al. 2013, ApJ, 774, 58
Eftekhari, T., Berger, E., Margalit, B., et al. 2019, ApJL, 876, L10
Eftekhari, T., Berger, E., Zauderer, B. A., Margutti, R., & Alexander, K. D. 2018, ApJ, 854, 86
Frohmaier, C., Sullivan, M., Maguire, K., & Nugent, P. 2018, ApJ, 858, 50
Frohmaier, C., Sullivan, M., Nugent, P. E., Goldstein, D. A., & DeRose, J. 2017, ApJS, 230, 4
Granot, J., & Sari, R. 2002, ApJ, 568, 820
Hinkle, J. T., Holoien, T. W. S., Shappee, B. J., et al. 2020, arXiv:2001.08215
Ho, A. Y. Q., Perley, D. A., Kulkarni, S. R., et al. 2020, arXiv:2003.01222
Ho, A. Y. Q., Phinney, E. S., Ravi, V., et al. 2019, ApJ, 871, 73
Holoien, T. W. S., Kochanek, C. S., Prieto, J. L., et al. 2016, MNRAS, 455, 2918
Hotokezaka, K., Kashiyama, K., & Murase, K. 2017, ApJ, 850, 18
Huang, Y. F., Dai, Z. G., & Lu, T. 2002, MNRAS, 332, 735
Jarrett, T. H., Cluver, M. E., Magoulas, C., et al. 2017, ApJ, 836, 182
Kalberla, P. M. W., Burton, W. B., Hartmann, D., et al. 2005, A&A, 440, 775
Kauffmann, G., Heckman, T. M., Tremonti, C., et al. 2003, MNRAS, 346, 1055
Kewley, L. J., & Dopita, M. A. 2002, ApJS, 142, 35
Kriek, M., van Dokkum, P. G., Labbé, I., et al. 2009, ApJ, 700, 221
Krolik, J., Piran, T., Svirski, G., & Cheng, R. M. 2016, ApJ, 827, 127
Kuin, N. P. M., Wu, K., Oates, S., et al. 2019, MNRAS, 487, 2505
Lang, D., Hogg, D. W., & Mykytyn, D. 2016, The Tractor: Probabilistic Astronomical Source Detection and Measurement, version dr8.1 (modified to model a point source superimposed on the galaxy), Astrophysics Source Code Library, ascl:1604.008
Law, C. J., Omand, C. M. B., Kashiyama, K., et al. 2019, ApJ, 886, 24
Law, N. M., Kulkarni, S., Ofek, E., et al. 2009, BAAS, 41, 418
Law-Smith, J., Ramirez-Ruiz, E., Ellison, S. L., & Foley, R. J. 2017, ApJ, 850, 22
Lazzati, D., Morsony, B. J., Blackwell, C. H., & Begelman, M. C. 2012, ApJ, 750, 68
Li, W., Bloom, J. S., Podsiadlowski, P., et al. 2011a, Natur, 480, 348
Li, W., Chornock, R., Leaman, J., et al. 2011b, MNRAS, 412, 1473
Lunnan, R., Chornock, R., Berger, E., et al. 2014, ApJ, 787, 138
Lyutikov, M., & Toonen, S. 2019, MNRAS, 487, 5618
MacFadyen, A. I., & Woosley, S. E. 1999, ApJ, 524, 262
MacFadyen, A. I., Woosley, S. E., & Heger, A. 2001, ApJ, 550, 410
Margutti, R., Kamble, A., Milisavljevic, D., et al. 2017a, ApJ, 835, 140
Margutti, R., Metzger, B. D., Chornock, R., et al. 2017b, ApJ, 836, 25
Margutti, R., Metzger, B. D., Chornock, R., et al. 2019, ApJ, 872, 18
Margutti, R., Milisavljevic, D., Soderberg, A. M., et al. 2014a, ApJ, 780, 21
Margutti, R., Milisavljevic, D., Soderberg, A. M., et al. 2014b, ApJ, 797, 107
Margutti, R., Soderberg, A. M., Wieringa, M. H., et al. 2013a, ApJ, 778, 18
Margutti, R., Zaninoni, E., Bernardini, M. G., et al. 2013b, MNRAS, 428, 729
Marleau, F. R., Clancy, D., & Bianconi, M. 2013, MNRAS, 435, 3085
Matheson, T., Filippenko, A. V., Chornock, R., Leonard, D. C., & Li, W. 2000, AJ, 119, 2303
Mattila, S., Pérez-Torres, M., Efstathiou, A., et al. 2018, Sci, 361, 482
McLeod, B., Fabricant, D., Nystrom, G., et al. 2012, PASP, 124, 1318
McMullin, J. P., Waters, B., Schiebel, D., Young, W., & Golap, K. 2007, in ASP Conf. Ser. 376, Astronomical Data Analysis Software and Systems XVI, ed. R. A. Shaw, F. Hill, & D. J. Bell (San Francisco, CA: ASP), 127
Meisner, A. M., Lang, D., & Schlegel, D. J. 2018, RNAAS, 2, 1
Mezcua, M., Civano, F., Marchesi, S., et al. 2018, MNRAS, 478, 2576
Michałowski, M. J., Gentile, G., Krühler, T., et al. 2018, A&A, 618, A104
Milisavljevic, D., Margutti, R., Kamble, A., et al. 2015, ApJ, 815, 120
Mohan, N., & Rafferty, D. 2015, PyBDSF: Python Blob Detection and Source Finder, version 1.8.9, Astrophysics Source Code Library, ascl:1502.007
Moriya, T. J., Mazzali, P. A., Tominaga, N., et al. 2017, MNRAS, 466, 2085
Nakar, E., & Piran, T. 2003, NewA, 8, 141
Nakar, E., & Sari, R. 2012, ApJ, 747, 88
Nava, L., Salvaterra, R., Ghirlanda, G., et al. 2012, MNRAS, 421, 1256
Nicholl, M., Berger, E., Smartt, S. J., et al. 2016, ApJ, 826, 39
Ofek, E. O., Rabinak, I., Neill, J. D., et al. 2010, ApJ, 724, 1396
Pasham, D. R., & van Velzen, S. 2018, ApJ, 856, 1
Perets, H. B., Gal-Yam, A., Mazzali, P. A., et al. 2010, Natur, 465, 322
Perley, D. A., Mazzali, P. A., Yan, L., et al. 2019, MNRAS, 484, 1031
Poznanski, D., Chornock, R., Nugent, P. E., et al. 2010, Sci, 327, 58
Prasad, J., & Chengalur, J. 2012, ExA, 33, 157
Prentice, S. J., Maguire, K., Smartt, S. J., et al. 2018, ApJL, 865, L3
Pursiainen, M., Childress, M., Smith, M., et al. 2018, MNRAS, 481, 894
Quimby, R. M., Yuan, F., Akerlof, C., & Wheeler, J. C. 2013, MNRAS, 431, 912
Rau, A., Kulkarni, S. R., Law, N. M., et al. 2009, PASP, 121, 1334
Readhead, A. C. S. 1994, ApJ, 426, 51
Rees, M. J. 1988, Natur, 333, 523
Reines, A. E., & Volonteri, M. 2015, ApJ, 813, 82
Rest, A., Garnavich, P. M., Khatami, D., et al. 2018, NatAs, 2, 307
Reynolds, T., Dong, S., Fraser, M., et al. 2016, ATel, 9645, 1
Rivera Sandoval, L. E., Maccarone, T. J., Corsi, A., et al. 2018, MNRAS, 480, L146
Chandra, P., & Frail, D. A. 2012, ApJ, 746, 156
Rybicki, G. B., & Lightman, A. P. 1979, Radiative Processes in Astrophysics (New York: Wiley-VCH)
Saxton, R. D., Read, A. M., Komossa, S., et al. 2017, A&A, 598, A29
Schlafly, E. F., & Finkbeiner, D. P. 2011, ApJ, 737, 103
Schulze, S., Krühler, T., Leloudas, G., et al. 2018, MNRAS, 473, 1258
Scott, M. A., & Readhead, A. C. S. 1977, MNRAS, 180, 539
Sedov, L. 1946, J. Appl. Math. Mech, 10, 241
Shappee, B., Prieto, J., Stanek, K. Z., et al. 2014, AAS Meeting, 223, 236.03
Shen, K. J., Kasen, D., Weinberg, N. N., Bildsten, L., & Scannapieco, E. 2010, ApJ, 715, 767
Shivvers, I., Zheng, W. K., Mauerhan, J., et al. 2016, MNRAS, 461, 3057
Skrutskie, M. F., Cutri, R. M., Stiening, R., et al. 2006, AJ, 131, 1163
Slysh, V. I. 1990, SvAL, 16, 339
Smith, N. 2014, ARA&A, 52, 487
Soderberg, A. M., Brunthaler, A., Nakar, E., Chevalier, R. A., & Bietenholz, M. F. 2010a, ApJ, 725, 922
Soderberg, A. M., Chakraborti, S., Pignata, G., et al. 2010b, Natur, 463, 513
Soderberg, A. M., Chevalier, R. A., Kulkarni, S. R., & Frail, D. A. 2006a, ApJ, 651, 1005
Soderberg, A. M., Kulkarni, S. R., Berger, E., et al. 2005, ApJ, 621, 908
Soderberg, A. M., Kulkarni, S. R., Nakar, E., et al. 2006b, Natur, 442, 1014
Strubbe, L. E., & Quataert, E. 2009, MNRAS, 400, 2070
Svensson, K. M., Levan, A. J., Tanvir, N. R., Fruchter, A. S., & Strolger, L. G. 2010, MNRAS, 405, 57
Tampo, Y., Tanaka, M., Maeda, K., et al. 2020, arXiv:2003.02669
Tan, J. C., Matzner, C. D., & McKee, C. F. 2001, ApJ, 551, 946
Tanaka, M., Tominaga, N., Morokuma, T., et al. 2016, ApJ, 819, 5
Tartaglia, L., Sand, D. J., Valenti, S., et al. 2018, ApJ, 853, 62
Taylor, G. 1950, RSPSA, 201, 159
van Eerten, H., van der Horst, A., & MacFadyen, A. 2012, ApJ, 749, 44
Vinkó, J., Yuan, F., Quimby, R. M., et al. 2015, ApJ, 798, 12
von Neumann, J. 1941, The Point Source Solution, U.S. Government Document AM-9, National Defense Research Council, Division B, Washington, DC
Whitesides, L., Lunnan, R., Kasliwal, M. M., et al. 2017, ApJ, 851, 107
Yang, S., Valenti, S., Cappellaro, E., et al. 2017, ApJL, 851, L48
Zauderer, B. A., Berger, E., Margutti, R., et al. 2013, ApJ, 767, 152
Zauderer, B. A., Berger, E., Soderberg, A. M., et al. 2011, Natur, 476, 425